Article:
Crann, CA, Patterson, RT, Macumber, AL et al. (5 more authors) (2015) Sediment accumulation rates in subarctic lakes: Insights into age-depth modeling from 22 dated lake records from the Northwest Territories, Canada. Quaternary Geochronology, 27. 131 - 144. ISSN 1871-1014

https://doi.org/10.1016/j.quageo.2015.02.001

Sediment accumulation rates in subarctic lakes: insights into age-depth modeling from 22 dated lake records from the Northwest Territories, Canada

Carley A. Crann[1]*[†], R. Timothy Patterson[1], Andrew L. Macumber[1], Jennifer M. Galloway[2], Helen M. Roe[3], Maarten Blaauw[3], Graeme T. Swindles[4], Hendrik Falck[5]

[1]Department of Earth Sciences and Ottawa-Carleton Geoscience Centre, Carleton University, Ottawa, Ontario, K1S 5B6, Canada

[2]Geological Survey of Canada Calgary/ Commission Géologique du Canada, Calgary, Alberta, T2L 2A7, Canada

[3]School of Geography, Archaeology and Palaeoecology, Queen's University, Belfast, Belfast, Northern Ireland, BT7 1NN, United Kingdom

[4]School of Geography, University of Leeds, Leeds, LS2 9JT, United Kingdom

[5]Northwest Territories Geoscience Office, Yellowknife, Northwest Territories, X1A 2R3, Canada

*Corresponding author: ccrann@uottawa.ca 613-562-5800 x6864

[†]Now: Department of Earth Sciences, University of Ottawa, Ottawa, Ontario, K1N 6N5, Canada

RTP: Tim.Patterson@carleton.ca
ALM: andrewmacumber@cmail.carleton.ca
JMG: jennifer.galloway@nrcan-rncan.gc.ca
HMR: h.roe@qub.ac.uk
MB: maarten.blaauw@qub.ac.uk
GTS: g.t.swindles@leeds.ac.uk
HF: hendrik_falck@gov.nt.ca

Abstract

Age-depth modeling using Bayesian statistics requires well-informed prior information about the behavior of sediment accumulation. Here we present average sediment accumulation rates (represented as deposition times, DT, in yr/cm) for lakes in an Arctic setting, and we examine the variability across space (intra- and inter-lake) and time (late Holocene). The dataset includes over 100 radiocarbon dates, primarily on bulk sediment, from 22 sediment cores obtained from 18 lakes spanning the boreal to tundra ecotone gradients in subarctic Canada. There are four to twenty-five radiocarbon dates per core, depending on the length and character of the sediment records. Deposition times were calculated at 100-year intervals from age-depth models constructed using the 'classical' age-depth modeling software Clam. Lakes in boreal settings have the most rapid accumulation (mean DT 20 ± 10 years), whereas lakes in tundra settings accumulate at moderate (mean DT 70 ± 10 years) to very slow rates, (>100 yr/cm). Many of the age-depth models demonstrate fluctuations in accumulation that coincide with lake evolution and post-glacial climate change. Ten of our sediment cores yielded sediments as old as c. 9,000 cal BP (BP = years before AD 1950). From between c. 9,000 cal BP and c. 6,000 cal BP, sediment accumulation was relatively rapid (DT of 20 to 60 yr/cm). Accumulation slowed between c. 5,500 and c. 4,000 cal BP as vegetation expanded northward in response to warming. A short period of rapid accumulation occurred near 1,200 cal BP at three lakes. Our research will help inform priors in Bayesian age modeling.

Keywords

Bayesian age-depth modeling, accumulation rate, deposition time, Bacon, Subarctic,

Northwest Territories, paleolimnology

1. Introduction

Lake sediment accumulation rates vary across space and time (Lehman, 1975; Terasmaa, 2011). Characterization of the spatial trends in accumulation rate for a region and within a lake basin is valuable for sample site selection in paleolimnological studies, as it is often favorable to sample lakes with sufficiently high accumulation rates to achieve a desirable temporal resolution in the data. Understanding the temporal variability and timing of major shifts in accumulation rate as well as the causes of major accumulation rate shifts for a region can be extremely valuable for deciding on levels in an age-depth model that would benefit from additional radiocarbon dates. Such changes in accumulation rate can be used to better understand the limnological system of study and the impact of climate change on that system. Moreover, there are many examples where changes in sediment accumulation rate have been linked to climatic change. For example, in the Cathedral Mountains of British Columbia, the highest Holocene levels of sediment yield are coincident with late Holocene (~ 4,000 BP) climate cooling, reduced catchment vegetation and increased terrestrial erosion (Evans and Slaymaker, 2004). Similarly, in a crater lake in equatorial East Africa, Blaauw et al. (2011) found that cooler climate conditions also resulted in reduced vegetation cover and increased terrestrial erosion and allochtonous sediment input into the lake. Knowledge of accumulation rate is also necessary for proxy-based reconstructions of mean fire return interval, rates of vegetation change (Koff et al., 2000; Marlon et al., 2006), and carbon accumulation rate studies (e.g. Charman et al. 2013), for example, that are only as good as the chronologies they are based upon.

77

78 The integration of sediment accumulation rate information into Bayesian age-depth
79 models as prior knowledge, or "priors" is particularly important for sections of an age-
80 depth model where the behavior of the model is uncertain (e.g. sparse data, age reversals,
81 age offsets, dates within a radiocarbon plateau). It can be a challenge, however, to
82 estimate the accumulation rate prior. Goring et al. (2012) provided a summary of
83 sediment accumulation rates from 152 lacustrine sites in the northeastern US/southeastern
84 Canada region and found that, in general, sediment accumulated with a DT of around 20
85 yr/cm. This result is fairly similar to the previous findings of Webb and Webb (1988; 10
86 yr/cm) for the same region. However, these estimates are too rapid for subarctic and
87 arctic lakes, where a short ice-free season and low availability of organic material relative
88 to more southern sites lead to slow annual sediment accumulation rates (e.g. Saulnier-
89 Talbot et al., 2009).

90

91 This paper expands upon the temperate lake research of Goring et al. (2012) and Webb
92 and Webb (1988). We examine Holocene accumulation rate data for 22 lacustrine sites
93 from a latitudinal gradient spanning boreal forest, treeline, and tundra settings in the
94 Northwest Territories, Canada. While this is a much smaller dataset than Webb and
95 Webb (1988) and Goring et al. (2012), it is significant given that it is logistically difficult
96 to obtain sediment records in arctic and subarctic regions due to the lack of infrastructure.
97 Goring et al. (2012) suggest that such regional datasets can provide important prior
98 knowledge to inform Bayesian (and other) age models.

99

The age-depth models presented in this paper were constructed in support of an interdisciplinary project aimed at better understanding the natural variability of climate along the routed of the Tibbitt to Contowyto Winter Road (TCWR) in the central Northwest Territories (Canada). Increased precision of age-depth models and increased sampling resolution of proxy data from lake sediment cores have permitted higher resolution characterization paleoclimate patterns (e.g., Galloway et al., 2010; Macumber et al., 2012; Upiter et al., 2014).

2. Regional setting

Lakes investigated in this study are located in the central Northwest Territories (Fig. 1) in an area underlain by a portion of the Canadian Shield known as the Slave Craton. This section of Archean crust is characterized by a depositional and volcanic history that has been overprinted by multiple phases of deformation and intruded by granitoid plutons (Bleeker, 2002). Major rock units include basement gneisses and metavolcanics, metasedimentary rocks, and widespread gneissic–granitoid plutons (Padgham and Fyson, 1992; Helmstaedt, 2009). This bedrock geology lacks carbon-rich rocks such as limestones or marl, and is unlikely to be a source of '^{14}C dead' carbon, which can cause radiocarbon dates to appear anomalously old.

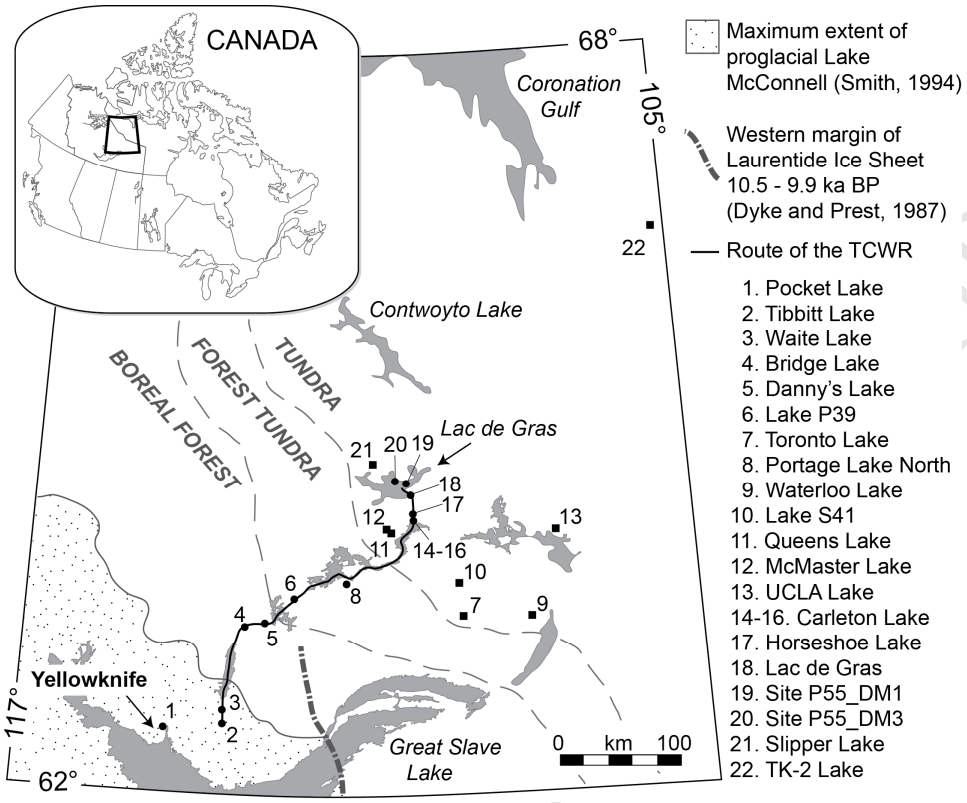

Figure 1. Map of the Northwest Territories showing the locations of core sites. Circles are sites from the TCWR project, squares are sites from previously published work, dashed lines show current boundaries between tundra, forest tundra, and boreal forest ecozones, and the inset shows the location of the study area within Canada. References for the previously published sites are given in Table 1. ***Two column image.***

The Slave Craton has been isostatically uplifting since the retreat of the Laurentide Glacier about 10,000–9,000 years ago (Dyke and Prest, 1987; Dyke et al., 2003). Glacial-erosional processes have shaped the terrain, which is characterized by a gentle relief of only a few tens of meters (Rampton, 2000). Where bedrock is not exposed, it lies beneath deposits of till and glaciofluvial sediment of varying thickness. The action

of glacial erosion and subglacial meltwater flow has resulted in a landscape with abundant, often interconnected lakes. Figure 1 shows the approximate western margin of the Laurentide Ice Sheet as it retreated toward the east, sometime between 10,500 and 9900 years ago (Dyke and Prest, 1987) as well as the maximum extent of proglacial Lake McConnell (Smith, 1994). Lake McConnell was the main proglacial lake in the region following the retreat of the Laurentide Ice Sheet.

The present-day treeline runs NW/SE across the study area, roughly reflecting the polar front (Fig. 1). The treeline is marked by the northern limits of the boreal forest (Fig. 2a), where forest stands are open and lichen woodlands merge into areas of shrub tundra (Galloway et al., 2010; Fig. 2b). Soils are poorly developed with discontinuous permafrost south of the treeline, and continuous permafrost north of the treeline (Clayton et al., 1977). Tundra vegetation is composed of lichens, mosses, sedges, grasses, and diverse herbs (MacDonald et al., 2009). The vegetation cover and soils are often affected by polygonal permafrost features (Fig. 2c), and are discontinuous on rocky substrates.

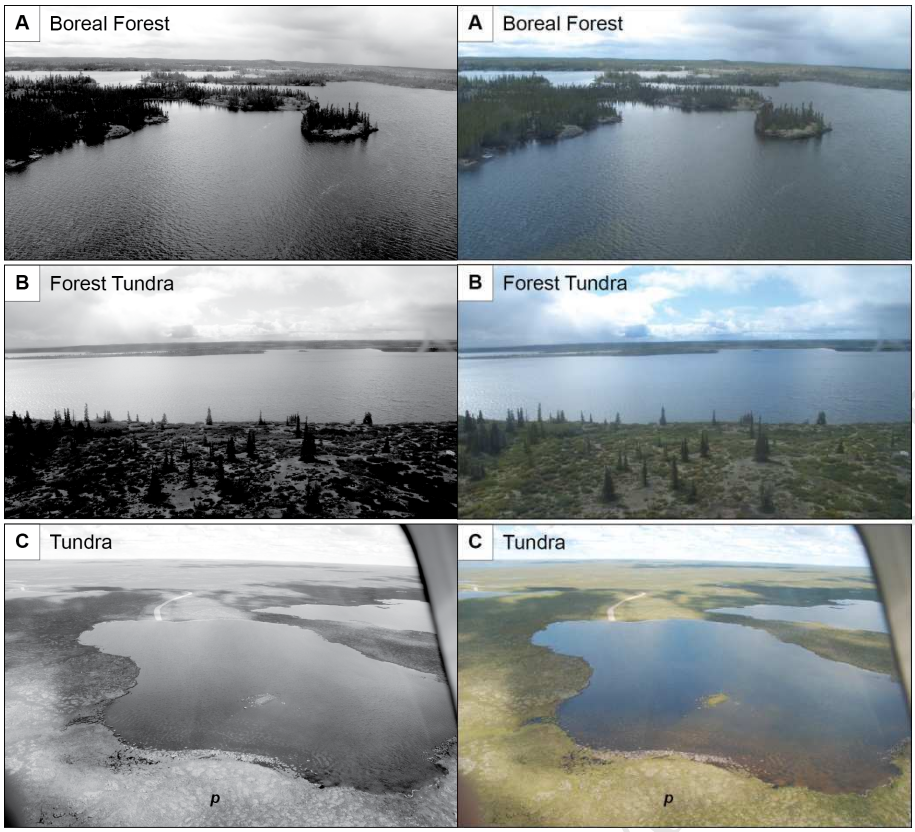

Figure 2. Images of the (a) boreal forest zone at Waite Lake, (b) forest tundra ecotone near Portage Lake North (actually Mackay Lake, not mentioned in this paper), and (c) tundra zone at Carleton Lake, where "p" shows an area with soil polygon development. At Carleton Lake, the path of the TCWR can be seen exiting the lake to the north. ***One column image. Colour version for web only. Black and white for print.***

The climate of the region is subarctic continental, characterized by short summers and long cold winters. Annual precipitation is low (175 – 200 mm) and mean daily January temperatures range from -17.5°C to -27.5°C, while mean daily July temperatures range from 7.5°C to 17.5°C. Lakes in the region are often ice-covered for much of the year, with an average open-water period of only 90 days (Wedel et al., 1990).

158 Broad-scale patterns of Holocene climate change in the study area have been identified
159 by proxy evidence from lake sediment cores from Toronto Lake (MacDonald et al., 1993;
160 Wolfe et al., 1996; Pienitz et al., 1999), Waterloo Lake (MacDonald et al., 1993), Lake
161 S41 (MacDonald et al., 2009), Queen's Lake (Moser and MacDonald, 1990; MacDonald
162 et al., 1993; Wolfe et al., 1996; Pienitz et al., 1999), McMaster Lake (Moser and
163 MacDonald 1990; MacDonald et al., 1993), UCLA Lake (Huang et al., 2004), Slipper
164 Lake (Rühland and Smol, 2005), and Lake TK-2 (Paul et al., 2010) (Fig. 1; Table 1).
165 Based on this body of previous work, three main stages of landscape development have
166 been inferred: (1) between deglaciation (c. 9,000 cal BP) and c. 6,000 cal BP, terrestrial
167 erosion decreased as vegetation developed from tundra to *Betula*-dominated shrub tundra,
168 and finally to spruce forest tundra (Huang et al., 2004; Sulphur et al., in prep) and
169 stabilized the landscape; (2) between c. 6,000 and c. 3,500 cal BP the treeline moved
170 north of its present location in response to climate warming (Moser and MacDonald,
171 1990; MacDonald et al., 1993), likely reflecting a northward retreat of the polar front
172 following the demise of the ice sheet in the middle Holocene (Huang et al., 2004); and (3)
173 between c. 3,000 cal BP to the present, there was a general trend towards climate cooling.
174 This resulted in an increase in birch-dominated shrub tundra in the more northerly sites
175 (UCLA lake; Huang et al., 2004). At the more southern locations, vegetation shifts
176 associated with climate change during the latest Holocene are also documented (change
177 c. 1,000 cal BP at Danny's Lake; Sulphur et al., in prep.).
178
179 **Table 1.** Coordinates and physical characteristics of the lakes used in this study.
180 Citations: (1) Moser and MacDonald, 1990; (2) MacDonald et al., 1993; (3) Edwards et

al., 1996; (4) Wolfe et al., 1996; (5) Penitz et al., 1999; (6) Huang et al., 2004; (7) Rühland and Smol, 2005; (8) MacDonald et al., 2009; (9) Paul et al., 2010; (10) Galloway et al., 2010; (11) Macumber et al., 2012; (12) Upiter et al., 2014.

*TCWR JV = Tibbitt to Contwoyto Winter Road Joint Venture

Site ID	Site name	TCWR JV* ID	Latitude	Longitude	Surface area (ha)	Depth (m)	Citation
1	Pocket Lake	-	62°30.540	114°22.314	6	3.5	
2	Tibbitt Lake	P0	62°32.800	113°21.530	300	6.72	10, 11
3	Waite Lake	P14-2	62°50.987	113°19.643	100	1.8	10, 11
4	Bridge Lake	P26	63°23.297	112°51.768	119.5	4.5	11
5	Danny's Lake	P34	63°28.547	112°32.250	4.4	4.4	11
6	Lake P39	P39	63°35.105	112°18.436	37.3	1.1	11
7	Toronto Lake	-	63°25.800	109°12.600	10	6.75	2, 4, 5
8	Portage Lake N	P47	63°44.538	111°12.957	194.9	4.85	11
9	Waterloo Lake	-	63°26.400	108°03.600	?	?	2
10	Lake S41	-	63°43.110	109°19.070	<0.3	4.4	8
11	Queens Lake	-	64°07.000	110°34.000	50	4.5	1–5
12	McMaster Lake	-	64°08.000	110°35.000	12	8.0?	1, 2
13	UCLA Lake	-	64°09.000	107°49.000	28	7.7	6
14	Carleton-1A	P49	64°15.571	110°05.878	29.8	15	11
15	Carleton-1B	P49	64°15.571	110°05.878	29.8	1.5	11, 12
16	Carleton-2012	P49	64°15.500	110°05.928	29.8	3.0	
17	Horseshoe Lake	P52	64°17.381	110°03.701	505	4.0	11
18	Lac de Gras	P55	64°25.794	110°08.168	~57 k	4.0	11
19	Lac de Gras_DM1	P55	64°30.393	110°15.255	~57 k	?	
20	Lac de Gras_DM3	P55	64°33.723	110°26.841	~57 k	?	
21	Slipper Lake	-	64°37.000	110°50.000	190	14.0	7
22	Lake TK-2	-	66°20.900	104°56.750	2.8	7.5?	9

3. Materials and methods

3.1 Core collection

The coordinates of each lake, as well as basic lake parameters (surface area, core depth, inlets/outlets) for each site and the relevant references are summarized in Table 1. Data from eight previously published paleolimnological studies located in the area have been incorporated into the dataset to improve perspective on regional trends. The sediment cores from these studies were collected using a modified Livingstone corer (Wright et al., 1984), except the Slipper Lake core, which was collected using a modified KB gravity

corer and a mini-Glew gravity corer (Glew, 1991; Glew et al., 2001).

Sampling sites were distributed across the boreal forest, forest-tundra, and tundra ecozones. Coring typically took place during the winter when equipment could be set up directly on the TCWR, thus limiting sites to lakes with winter road access. Water depth was measured in the field using a fish finder (echo sounder). For five lakes, detailed bathymetric profiles were provided by EBA Engineering Consultants Ltd. These profiles were collected during a through-ice bathymetry survey using ground-penetrating radar (GPR) towed behind a vehicle.

The 14 new cores were collected using 1.5-2.0 m long, 10-20 cm wide, freeze corers (hollow, metal-faced corers filled with dry ice; Galloway et al., 2010; Macumber et al., 2012). Freeze corers are ideal for the extraction of cores in unconsolidated and water-saturated sediment as they capture sediment by *in situ* freezing (Lotter et al., 1997; Glew et al., 2001; Kulbe and Niederreiter, 2003; Blass et al., 2007). In 2009, Tibbitt and Waite lakes were cored using a single-sided freeze corer (Galloway et al., 2010). The uppermost sediments from the Waite Lake coring site were unfortunately not recovered as the freeze corer over-penetrated the sediment-water interface during sampling. A Glew core (Glew, 1991) was collected in 2011 in an attempt to capture the missing sediment-water interface. In 2010 a custom designed double-sided freeze corer was deployed in addition to the single-faced corer, to increase the volume of sediment obtained at a given site (Macumber et al., 2012). Freeze cores were sliced at millimeter-scale resolution using a custom designed sledge microtome (Macumber et al., 2011). The

highest sampling resolution previously reported previously reported for the region had been half-centimeter intervals from the Slipper Lake (Rühland and Smol, 2005) and Lake S41 cores (MacDonald et al., 2009).

3.2 Chronology

With the exception of one twig date in each of the Waite Lake and Queen's Lake cores, and four twig dates in the Lake TK-2 core, radiocarbon dates were obtained from bulk sediment samples, as macrofossils were not encountered during screening. Samples were pretreated with a standard acid wash to remove carbonate material, and unless otherwise stated in Section 4, analyses were performed using the accelerator mass spectrometer (AMS) at the ^{14}Chrono Dating Laboratory at Queen's University Belfast. Radiocarbon dates reported from previous work employed both conventional and AMS techniques. All radiocarbon ages in were calibrated using either Clam (Blaauw, 2010) or Calib software version 6.1.0 (Stuiver and Reimer, 1993); both programs used the IntCal09 calibration curve (Reimer et al., 2009). Radiocarbon ages younger than AD1950 were calibrated in CALIBomb (Reimer et al., 2004) with the NH_zone1.14c dataset (Hua and Barbetti, 2004). For the Holocene dates used in this study, the differences between the IntCal09 and IntCal13 (Reimer et al., 2013) calibration curves, as well as between the 2004 and 2013 (Hua et al., 2013) postbomb curves are negligible (for our purposes), but we would recommend using the newest curves in future studies. Dates from a ^{210}Pb profile from Slipper Lake were also incorporated into the dataset (Rühland and Smol, 2005). The Pocket Lake core contains a visible tephra layer, which was geochemically confirmed to as part of the White River Ash deposit (Crann et al., in prep). This horizon

240 will be used in future studies to further constrain the age-depth model. The core from
241 nearby Bridge Lake was analyzed for both visible and cryptotephra, but was unsuccessful
242 in finding evidence for deposition of the White River Ash.
243
244 *3.3 Classical age-depth modeling with Clam*
245 Smooth spline age-depth models were constructed for sediment cores obtained from the
246 TCWR and previously published studies using the 'classical' age-depth modeling
247 software Clam (Blaauw, 2010, R statistical software package) and the IntCal09
248 calibration curve (Reimer et al., 2009). The year the core was collected was added as the
249 age of the sediment-water interface with an error of ±5 years. The smoothing parameter,
250 which controls how sharply the model will curve toward radiocarbon dates, was
251 increased from the default value of 0.3 to 0.7 for the Danny's Lake model and to 0.5 for
252 the Waite Lake model in order to increase smoothness of the models through the large
253 number of radiocarbon dates. Otherwise, Clam's default smoothing parameter of 0.3 was
254 employed. The core from Lake P39 had only three non-outlying (see next paragraph)
255 dated horizons so the model was constructed using a linear regression. For Slipper Lake,
256 the three uppermost non-interpolated ^{210}Pb dates were included in the model.
257
258 For cores with low dating resolution (typically less than five radiocarbon dates or less
259 than one radiocarbon date per thousand years), suspected outliers were removed on an ad
260 hoc basis when a radiocarbon date either created a clear age reversal in the model or an
261 anomalous shift in accumulation rate that could not be supported by sedimentological
262 evidence (visible colour change from grey clay to dark green-brown sediment). We also

263 took into account the regional trends in sediment accumulation rate to aid with outlier
264 identification. For example, many age-depth models show a pronounced decrease in
265 accumulation rate after about 6,000 or 5,000 cal BP.
266
267 The Danny's Lake core is 115 cm long and has a few age reversals among the 25-
268 radiocarbon dates. A Bayesian outlier analysis was performed using the general outlier
269 model (Bronk Ramsey, 2009a) on a sequence in OxCal version 4.1 (Bronk Ramsey,
270 2009b). This model assumes that the dates are ordered chronologically (dates further
271 down having older ages) and that outliers are in the calendar time dimension and
272 distributed according to a Student-*t* distribution with 5 degrees of freedom (Christen,
273 1994; Bronk Ramsey, 2009a). Each radiocarbon date was assigned a 5% prior
274 probability of being an outlier. The first outlier analysis identified all three dates at the
275 bottom of the core as outliers so we increased the prior probability of UBA-16439 to
276 10%, as this date created the largest age reversal. A subsequent outlier analysis still
277 identified the two bottommost dates as outliers and it was unclear as to which was more
278 likely to be an outlier. We then examined the age-depth models from other lakes and
279 from previous studies for clues to resolve this problem. As many of the other models
280 support a higher accumulation rate prior to about 6000 cal BP we used this information to
281 increase the prior probability of UBA-17932 being an outlier to 10%. In Section 5, we
282 show how the Bayesian software Bacon produces age models without performing a
283 separate, formal outlier analysis.
284
285 *3.4 Estimation of deposition time (DT)*

An estimate of DT (yr/cm, inverse of accumulation rate) is required as *a priori* information to generate age-depth models using the Bayesian software Bacon (Blaauw and Christen, 2011). This estimate can be based on prior knowledge obtained from previously built age-depth models from lakes in the region (Goring et al., 2012). Here we generate a summary for the region using the age-depth models constructed in Clam to calculate the DT at 100-year intervals for each model. It should be noted that the intention of the summary is to produce initial estimates of DT for age-depth modeling and the data has not undergone a rigorous statistical analysis. The DT between the uppermost non-outlying date and the date used to model the surface age were not included in graphing the accumulation rates because: (1) there is potential uncertainty with the assumption that the age of the sediment-water interface is indeed the year that the core was collected; and (2) high water content in the uppermost sediments can lead to an anomalously rapid DT. Webb and Webb (1988) assumed 50% compaction in sediments below the uppermost 5 to 10 cm of the sediment column based on dry weight/wet weight ratios, yet they found that the accumulation rates were still higher during the historic period. Because dry weight/wet weight data has not been collected for this study, the effect of compaction and dewatering is not taken into account in graphing the DT. P39 and Slipper lake cores lacked sufficient chronological control and were omitted from the DT compilation dataset.

4. Results

The radiocarbon dates from all sites included in this study, along with the results from the outlier analysis, are summarized in Table 2. The age-depth models constructed using

Clam have been grouped into three categories (Fig. 3). The first category, rapid sediment accumulation rate lakes, contains five age-depth models that stand out from the rest. Deposition times in this category do not tend to exceed 50 yr/cm, and the average DT (rounded to the nearest 10 = 20 yr/cm) is on par with lakes in the Great Lakes region (Goring et al., 2012). The other two categories, moderate and slow sediment accumulation rate lakes, are not so easily distinguished. Accumulation rates for age-depth models in both categories fluctuate, but moderate sediment-rate accumulating sites tend to fluctuate at more subtle amplitudes (DT of around 50 yr/cm) and do not often exceed a DT of 100 yr/cm. Sites with overall slow accumulation rates fluctuate with DT amplitudes up to 150 yr/cm, and tend to be in excess of 100 yr/cm.

Detailed results for each category are given in Sections 4.1-4.3. Because these results are intended to yield insight into the spatial and temporal variability in accumulation rates in high latitude lakes and to give estimates of DT that can be used as prior information in Bayesian age-depth modeling with Bacon, DTs are rounded to the nearest 10 yr/cm.

Table 2. Radiocarbon ages from all sites, calibrated with the IntCal09 calibration curve (Reimer et al., 2009) using either Calib software version 6.1.0 (Stuiver and Reimer, 1993) or Clam (Blaauw, 2010). The radiocarbon ages younger than AD1950 (italics) were calibrated in CALIBomb (Reimer et al., 2004) with the NH_zone 1.14c dataset (Hua and Barbetti, 2004). The year the core was collected is included as it was used to model the age of the sediment-water interface in the Clam age-depth models. Dates identified as outliers are shown in bold and radiocarbon dates younger than AD1950 are in italics.

Lake information	Lab ID	Method	Depth (cm)	^{14}C age (BP) ± 1σ	Material dated	Cal BP ± 2σ
Pocket Lake	UBA-20676	AMS	10–10.5	362 ± 27	Bulk	310–414
collected in 2012	UBA-22350	AMS	20–20.5	731 ± 31	Bulk	653–727
Freeze core (2F_F1)	UBA-20679	AMS	52–52.5	1335 ± 25	Bulk	1286–1383
	UBA-22351	AMS	57–57.5	1394 ± 30	Bulk	1279–1348
	UBA-22352	AMS	70–70.5	1725 ± 31	Bulk	1556–1708
	UBA-20677	AMS	90–90.5	2501 ± 30	Bulk	2443–2559
	UBA-22353	**AMS**	**110–110.5**	**1516 ± 35**	**Bulk**	**1333–1518**
	UBA-20678	AMS	128.5–129	2966 ± 26	Bulk	2916–3016
Tibbitt Lake (P0)	UBA-17353	AMS	20–21	67 ± 22	Bulk	(-4)–255
collected in 2009	UBA-17354	AMS	40–41	1409 ± 20	Bulk	1292–1343
Freeze core (1FR)	UBA-17355	AMS	80–81	2046 ± 26	Bulk	1930–2111
	Beta-257687	AMS	138–138.5	2390 ± 40	Bulk	2338–2696
Waite Lake (P14-2)	*UBA-18968*	*AMS*	*17–17.5*	*1.0562 ±0.003*	*Bulk*	*AD1956–1957*
collected in 2010	UBA-18969	AMS	27–27.5	309 ± 22	Bulk	304–455
Glew core	UBA-18970	AMS	37–37.5	556 ± 26	Bulk	522–637
Waite Lake (P14-2)	UBA-18474	AMS	0	1084 ± 41	Bulk	927–1066
collected in 2009	UBA-16433	AMS	16.9	995 ± 24	Bulk	800–961
Freeze core (1FR)	UBA-16434	AMS	29.1	1129 ± 22	Bulk	965–1076
	UBA-16435	AMS	43.2	1455 ± 23	Bulk	1304–1384
	UBA-16436	AMS	57.8	1519 ± 22	Bulk	1345–1514
	Beta-257686	AMS	66.3	1520 ± 40	Bulk	1333–1520
	UBA-15638	AMS	109.7	2107 ± 29	Twig	1997–2149
	Beta-257688	AMS	154	2580 ± 40	Bulk	2498–2769
	Beta-257689	AMS	185	2920 ± 40	Bulk	2955–3210
	Beta-257690	AMS	205.1	3460 ± 40	Bulk	3633–3838
Bridge Lake (P26-1)	UBA-18964	AMS	6.5–7	28 ± 23	Bulk	(-4)–244
collected in 2010	UBA-22873	AMS	12.5–13	694 ± 26	Bulk	565–683
Freeze core (2F_F2)	UBA-18965	AMS	18–18.5	1883 ± 23	Bulk	1736–1882
	UBA-22874	AMS	24.5–25	3782 ± 30	Bulk	4082–4246
	UBA-22875	AMS	30.5–31	4730 ± 30	Bulk	5326–5583
	UBA-22876	AMS	34.5–35	5487 ± 31	Bulk	6210–6322
	UBA-18966	AMS	41.5–42	5816 ± 42	Bulk	6501–6727
	UBA-22877	AMS	50.5–51	6184 ± 32	Bulk	6977–7172
	UBA-18967	AMS	59.5–60	6762 ± 32	Bulk	7576–7667
	UBA-22878	AMS	64–64.5	7025 ± 34	Bulk	7788–7941
Danny's Lake (P34-2)	UBA-17359	AMS	5.7	693 ± 21	Bulk	567–679
collected in 2010	UBA-17360	AMS	10.2	855 ± 23	Bulk	695–795
Freeze core (2F_F2)	UBA-16543	AMS	15–15.5	1329 ± 23	Bulk	1184–1299
	UBA-17361	AMS	21.9	1617 ± 25	Bulk	1416–1556
	UBA-17431	AMS	27.8	1659 ± 21	Bulk	1521–1615
	UBA-16544	AMS	32.6	1916 ± 25	Bulk	1818–1904
	UBA-20377	AMS	33.5	2071 ± 24	Bulk	1987–2120
	UBA-20378	AMS	34.2	2159 ± 24	Bulk	2061–2305
	UBA-17929	AMS	34.5	2257 ± 26	Bulk	2158–2343

Lake information	Lab ID	Method	Depth (cm)	^{14}C age (BP) ± 1σ	Material dated	Cal BP ± 2σ
	UBA-20376	**AMS**	**35.3**	**2073 ± 28**	**Bulk**	**1986–2124**
	UBA-20375	AMS	36.8	2248 ± 25	Bulk	2158–2339
	UBA-17432	**AMS**	**37.6**	**2659 ± 32**	**Bulk**	**2742–2884**
	UBA-20374	AMS	38.4	2392 ± 25	Bulk	2345–2488
	UBA-20373	AMS	39.3	2448 ± 33	Bulk	2358–2702
	UBA-17930	AMS	40.4	2549 ± 26	Bulk	2503–2748
	UBA-20371	AMS	41.4	2554 ± 28	Bulk	2503–2750
	UBA-20372	**AMS**	**43.3**	**4863 ± 29**	**Bulk**	**5583–5652**
	UBA-16545	AMS	45–45.5	2912 ± 24	Bulk	2964–3157
	UBA-16546	AMS	56.9	3604 ± 25	Bulk	3845–3975
	UBA-16547	AMS	70.1	5039 ± 51	Bulk	5661–5903
	UBA-16548	AMS	85–85.5	5834 ± 29	Bulk	6560–6733
	UBA-17931	AMS	89.5	6231 ± 34	Bulk	7016–7253
	UBA-16439	**AMS**	**95.5**	**8112 ± 32**	**Bulk**	**8997–9125**
	UBA-17932	**AMS**	**99.1**	**7623 ± 38**	**Bulk**	**8370–8518**
	UBA-16440	AMS	113.6	7450 ± 30	Bulk	8191–8346
P39-1A	**UBA-17344**	**AMS**	**10–10.5**	**3597 ± 26**	**Bulk**	**3840–3973**
collected in 2010	UBA-17345	AMS	19–19.5	3701 ± 24	Bulk	3974–4144
Freeze core (2F_F1)	UBA-17346	AMS	29–29.5	5385 ± 35	Bulk	6018–6284
Toronto Lake	Beta-49705	conv.	35–50	1760 ± 90	Bulk	1421–1887
collected in 1987	Beta-53129	conv.	80–85	4200 ± 80	Bulk	4450–4956
Livingstone core	Beta-53130	conv.	125–130	5460 ± 90	Bulk	6001–6408
	Beta-49708	conv.	155–160	7040 ± 120	Bulk	7657–8155
Portage Lake N. (P47-1)	UBA-17933	AMS	6.5–7	772 ± 24	Bulk	673–729
collected in 2010	UBA-17159	AMS	13.5–14	4218 ± 38	Bulk	4626–4854
Freeze core (2F_F2)	**UBA-17160**	**AMS**	**41–41.5**	**4885 ± 37**	**Bulk**	**5584–5710**
	UBA-17161	AMS	63–63.5	5333 ± 35	Bulk	5997–6264
	UBA-17162	AMS	86.5–87	5878 ± 34	Bulk	6637–6783
Waterloo Lake	**TO-3312**	**AMS**	**28–31**	**4030 ± 50**	**Bulk**	**4413–4801**
collected in 1987?	TO-3311	AMS	54–56	4640 ± 50	Bulk	5090–5577
Livingstone core	TO-3310	AMS	61–63.5	5300 ± 50	Bulk	5939–6257
	TO-3313	AMS	75–77	7640 ± 100	Moss	8206–8627
Lake S41	UCI-25833	AMS	7–7.5	375 ± 15	Bulk	331–499
collected in 2005	UCI-25841	AMS	13.4–14	1045 ± 20	Bulk	926–1042
Livingstone core	UCI-25836	AMS	23–23.5	1985 ± 15	Bulk	1892–1987
	UCI-25835	AMS	32.5–33	2765 ± 20	Bulk	2789–2924
Queen's Lake	WAT-1770	conv.	15–20	3820 ± 60	Bulk	4010–4414
collected in 1987?	WAT-1771	conv.	45–50	5600 ± 60	Bulk	6291–6493
Livingstone core	WAT-1772	conv.	60–65	6150 ± 60	Bulk	6888–7241
	WAT-1773	conv.	100–105	7150 ± 70	Bulk	7842–8159
	TO-827	AMS	105	7470 ± 80	Twig	8060–8417
McMaster Lake	**TO-766**	**AMS**	**10–12**	**3690 ± 50**	**Bulk**	**3888–4212**
collected in 1987?	TO-158	AMS	20–22	3680 ± 60	Bulk	3849–4220
Livingstone core	TO-767	AMS	30–32	5120 ± 60	Bulk	5730–5990

Lake information	Lab ID	Method	Depth (cm)	^{14}C age (BP) ± 1σ	Material dated	Cal BP ± 2σ
	TO-156	AMS	40–42	5360 ± 60	Bulk	5998–6279
	TO-154	AMS	60–62	6180 ± 60	Bulk	6943–7248
UCLA Lake	TO-8840	AMS	20–21	2370 ± 50	Bulk	2319–2698
Livingstone core	TO-8842	AMS	35–35.5	4130 ± 50	Bulk	4527–4824
	TO-8844	AMS	45–45.5	5680 ± 70	Bulk	6317–6635
	TO-8845	AMS	50–50.5	6280 ± 70	Bulk	7002–7413
	TO-8846	AMS	55.5–56	7040 ± 70	Bulk	7707–7978
	TO-8847	AMS	64.5–65	7680 ± 70	Bulk	8382–8590
	TO-8848	AMS	69.5–70	7960 ± 80	Bulk	8605–9006
Carleton Lake (P49-1A)	**UBA-19464**	**AMS**	**9.5–10**	**2794 ± 34**	**Bulk**	**2791–2970**
collected in 2010	**UBA-20002**	**AMS**	**15–15.5**	**2778 ± 26**	**Bulk**	**2793–2950**
Freeze core (2F_F2)	UBA-20003	AMS	25–25.5	2716 ± 33	Bulk	2757–2868
	UBA-19465	AMS	32.5–33	3124 ± 41	Bulk	3254–3443
	UBA-19466	AMS	40.5–41	3616 ± 37	Bulk	3835–4075
	UBA-19467	AMS	66.5–67	4927 ± 38	Bulk	5594–5728
Carleton Lake (P49-1B)	*UBA-18472*	*AMS*	*0–0.5*	*1.0264 ± 0.0035*	*Bulk*	*AD1955-1957*
collected in 2010	UBA-17934	AMS	10–10.5	1046 ± 24	Bulk	925–983
Freeze core (1F)	UBA-17347	AMS	19.5–20	1925 ± 25	Bulk	1822–1926
	UBA-17935	AMS	40–40.5	2762 ± 35	Bulk	2780–2946
	UBA-17348	AMS	64.5–65	3675 ± 24	Bulk	3926–4087
	UBA-17936	AMS	80–80.5	4635 ± 32	Bulk	5304–5465
	UBA-17349	AMS	100–100.5	5663 ± 26	Bulk	6399–6497
Carleton Lake (R12-P49)	UBA-20612	AMS	10.0	702 ± 39	Bulk	560–699
collected in 2012	UBA-20613	AMS	36.2	1337 ± 31	Bulk	1181–1305
Freeze core (2F_F2)	UBA-20614	AMS	55.3	1302 ± 46	Bulk	1132–1304
	UBA-20615	AMS	81.5	2132 ± 31	Bulk	2002–2299
	UBA-20616	AMS	117.8	2944 ± 32	Bulk	2989–3216
Horseshoe Lake (P52-1)	UBA-17350	AMS	9–9.5	178 ± 25	Bulk	(-2)–291
collected in 2010	UBA-17163	AMS	18–18.5	1148 ± 42	Bulk	967–1172
Freeze core (2F_F2)	UBA-17351	AMS	28–28.5	2763 ± 22	Bulk	2785–2924
	UBA-17352	AMS	38–38.5	3343 ± 23	Bulk	3481–3639
	UBA-19973	AMS	43.2	3776 ± 36	Bulk	3992–4281
	UBA-17938	AMS	46–46.5	4885 ± 27	Bulk	5589–5653
	UBA-17165	AMS	55–55.5	5916 ± 58	Bulk	6628–6897
	UBA-17937	AMS	68–68.5	6723 ± 29	Bulk	7516–7656
	UBA-17166	AMS	80–80.5	7488 ± 40	Bulk	8199–8383
	UBA-17167	AMS	106–106.5	8011 ± 43	Bulk	8718–9014
Lac de Gras (LDG)	UBA-17939	AMS	12–12.5	1123 ± 23	Bulk	965–1067
collected in 2010	**UBA-17356**	**AMS**	**19–19.5**	**3299 ± 38**	**Bulk**	**3447–3631**
Freeze core (2F_F2)	UBA-17357	AMS	32–32.5	1607 ± 29	Bulk	1412–1551
	UBA-17358	AMS	46–46.5	2144 ± 35	Bulk	2003–2305
Lac de Gras (LDG_DM1)	D-AMS 001550	AMS	10–11	784 ± 23	Bulk	677–732
collected in 2012	D-AMS 001551	AMS	20–21	1797 ± 23	Bulk	1629–1817
Freeze core	D-AMS 001552	AMS	30–31	2636 ± 25	Bulk	2738–2781
	D-AMS 001553	AMS	40–41	3590 ± 27	Bulk	3836–3972
Lac de Gras (LDG_DM3)	D-AMS 001554	AMS	10–11	1719 ± 23	Bulk	1561–1696

Lake information	Lab ID	Method	Depth (cm)	^{14}C age (BP) ± 1σ	Material dated	Cal BP ± 2σ
collected in 2012	D-AMS 001555	AMS	20–21	3459 ± 26	Bulk	3642–3828
Freeze core	D-AMS 001556	AMS	30–31	5509 ± 28	Bulk	6223–6396
	D-AMS 001557	AMS	40–41	7827 ± 31	Bulk	8543–8696
Slipper Lake	^{210}PB Age	n/a	0	n/a	Bulk	(-49)–(-45)
collected in 1997	^{210}PB Age	n/a	2	n/a	Bulk	6–20
KB gravity and mini-Glew	^{210}PB Age	n/a	3	n/a	Bulk	34–94
	TO-9671	AMS	21.5–22.5	3270 ± 80	Bulk	3359–3688
	TO-9672	AMS	43.5–44.5	4760 ± 70	Bulk	5321–5603
Lake TK-2	Beta-167871	AMS	32–34	2480 ± 40	Bulk	2365–2718
collected in 1996	Beta-167872	AMS	60–62	3870 ± 40	Bulk	4157–4416
Livingstone core	Beta-167873	AMS	96–98	5670 ± 40	Bulk	6322–6558
	TO-7871	AMS	132	7370 ± 80	Twigs	8020–8349
	TO-7870	AMS	137	7190 ± 80	Twigs	7860–8178
	TO-7869	AMS	142	7740 ± 90	Twigs	8375–8772
	TO-7868	AMS	174	7780 ± 70	Twigs	8412–8761

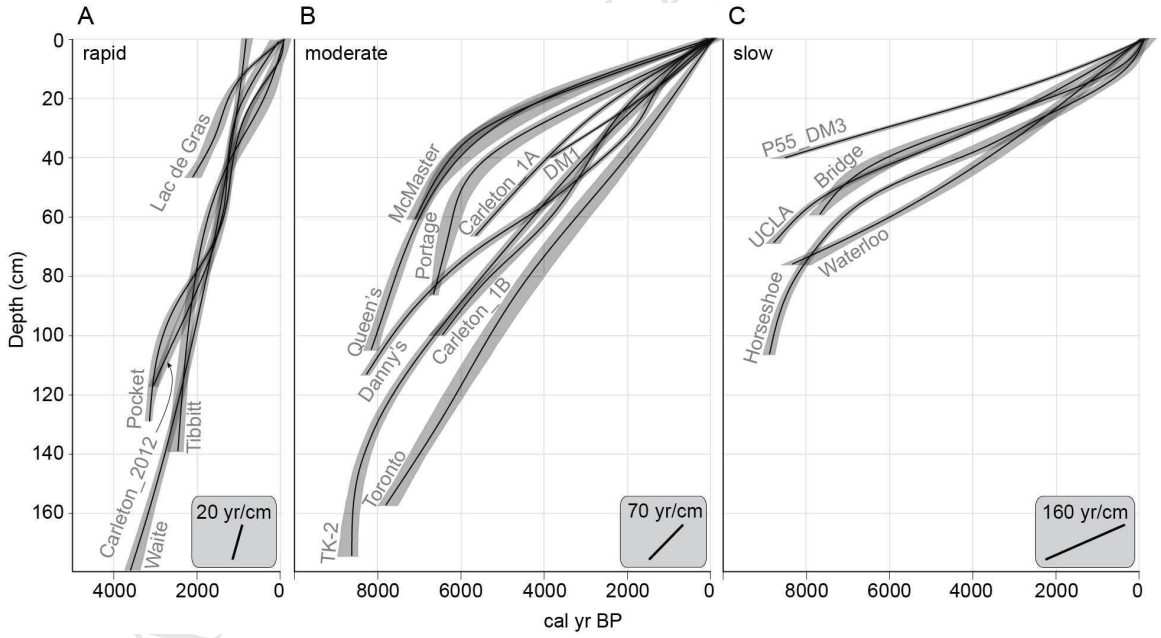

Figure 3. Age-depth models constructed using a smooth spline regression in Clam, grouped into (a) rapid, (b) moderate, and (c) slowly accumulating sites. The 95% confidence interval is light grey. The scale for Waite Lake is to be used as a relative measure only as the freeze corer over-penetrated the sediment-water interface. ***Two***

column image.

4.1 Sites with rapid accumulation rates (DT<50 yr/cm)

Rapid sediment accumulation rates are defined as having the DT for the majority of the core of less than 50 yr/cm. Five distinctive age depth models belonging to this category were produced for cores from Lac de Gras, Pocket, Tibbitt, Waite and Carleton lakes. Due to rapid sediment accumulation rates, these core records tend to span ~3,500 years at most. The cores in this category yielded internally consistent age-depth models, with the exception of one radiocarbon date that is a clear outlier in the Lac de Gras core (Table 2). The average DT (rounded to the nearest 10 = 20 yr/cm) is on par with lakes in the Great Lakes region (Goring et al., 2012).

Deposition times in these lakes vary between c. 10 and 50 yr/cm, with a mean of c. 20±10 yr/cm (1σ) and a unimodal distribution, based on 107 DT measurements at 100-year intervals (Fig. 4a). The accumulation pattern for Tibbitt Lake is different from the others as it increases steadily from a DT of c. 5 yr/cm at c. 2,500 cal BP to c. 50 yr/cm at the top, but the very rapid deposition near the base overlaps the Hallstatt Plateau (c. 2,700-2,300 cal BP; Blockley et al., 2007), which is a flat section in the IntCal09 calibration curve and therefore may be an artifact of calibration.

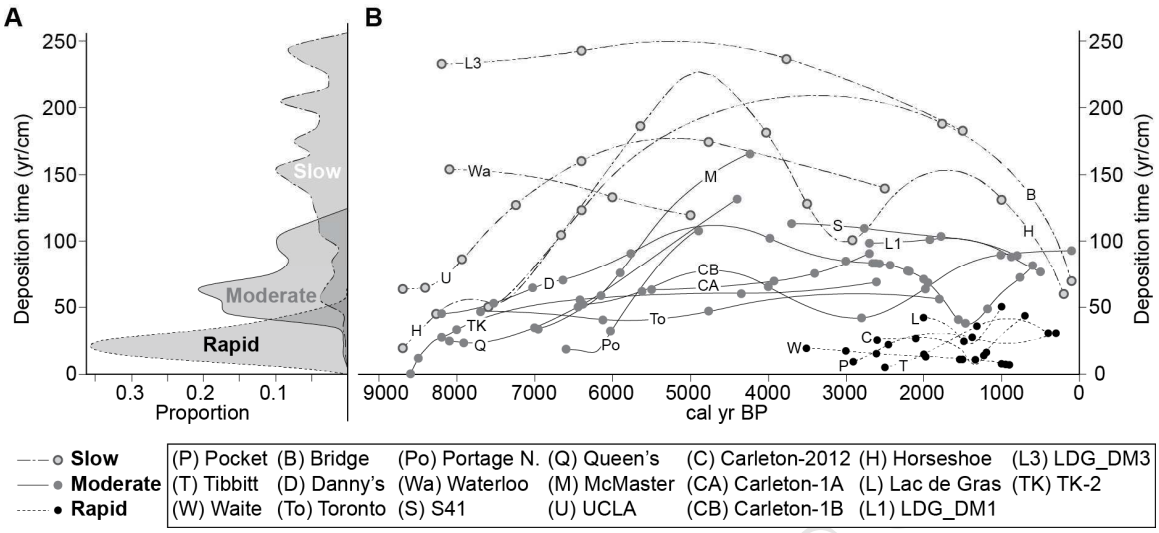

358

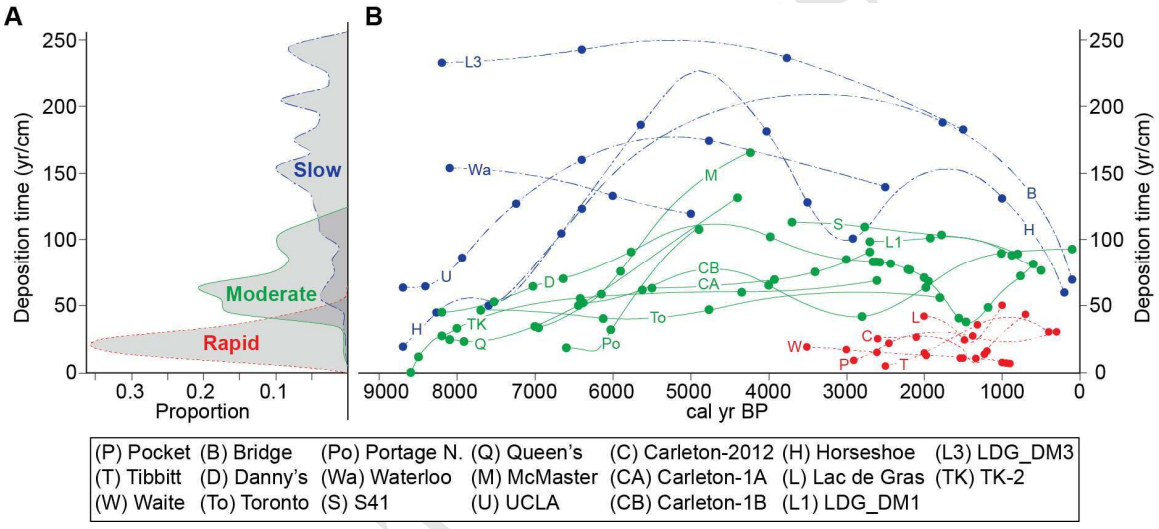

359

360 **Figure 4.** (a) Histogram of DT from rapid, moderate, and slowly accumulating lake site
361 categories, sampled at 100-year intervals from the age-depth models constructed in clam.
362 (b) Accumulation rate profiles for each site showing fluctuation of DT over time and the
363 variability between lake sites. The dots correspond to radiocarbon dates. ***Two column***
364 ***image. Colour version for web only. Black and white for print.***

365

366 *4.2 Sites with moderate accumulation rates (DT 50 – 100 yr/cm)*

367 The distinguishing characteristics of sites within this category include fluctuations in

368 sediment accumulation rate at relatively subtle amplitudes (DT around 50 yr/cm) and
369 DTs that do not generally exceed 100 yr/cm. The sites in this category are Danny's,
370 Toronto, S41, Carleton-1A, Carleton-1B, LDG_DM1, and TK-2. Three of the cores in
371 the moderate accumulation rate category are characterized by a sedimentary record that
372 extends just beyond 8,000 cal BP. The other four cores in this category have records that
373 extend back between c. 6,000 and c. 4,000 cal BP (Fig. 3).
374
375 The outlier analysis performed in OxCal identified five outliers in the Danny's Lake core,
376 which were omitted from the smooth spline age-depth model constructed with Clam.
377 Four of the five outliers were older than the model and the fifth was only slightly
378 younger. For Carleton-1A, the upper three radiocarbon dates, at 9.5, 15 and 25 cm, all
379 overlapped within the age range of c. 2,900 to c. 2,700 cal BP. For this reason the
380 uppermost two dates were omitted from the age-depth model constructed in Clam. The
381 overlap may have been the result of sediment mixing. The core from Lake TK-2 has an
382 age reversal within the bottommost four dates. Because these dates were obtained from
383 twigs (allochthonous origin and lack of heartwood), the reversal is likely due to delayed
384 deposition of older organic material. Clam was able to accept the reversal as the date was
385 within error of the others.
386
387 The lakes in this category accumulated with DTs between 50 and 100 yr/cm with a mean
388 of c. 70±20 yr/cm (1σ) based on 343 DT measurements at 100-year intervals (Fig. 4).
389 The histogram shown in figure 4a has a bimodal distribution with a primary mode around
390 60 yr/cm and a secondary mode around 100 yr/cm. Most of the lakes in this category

391 exhibit fluctuations in accumulation rate over time.

392

393 *4.3 Sites with slow accumulation rates (DT 100 – 250 yr/cm)*

394 Accumulation rates fluctuate in age-depth models for lakes with moderate and slow rates,
395 producing some overlapping characteristics. Sites with overall slow accumulation rates
396 fluctuate with DT amplitudes up to 150 yr/cm that tend to exceed 100 yr/cm. The sites in
397 the slow accumulation category are Bridge, Waterloo, UCLA, Horseshoe, and
398 LDG_DM3. All five sites in this category extend back to at least c. 8000 cal BP or
399 beyond. The age-models are internally consistent, with only one outlier identified from
400 the Waterloo Lake age-depth model, where the age is older than the model (Fig. 3).

401

402 The histogram of DTs (Fig. 4a) is multi-modal, reflecting high variability of sediment
403 accumulation rates for cores within this category. The main pattern occurs between about
404 8,000 and 5,000 cal BP, where Bridge, UCLA, and Horseshoe lakes are all characterized
405 by a slowing of accumulation rate (increased DT). This rate change is coincident with
406 changes in sedimentation from minerogenic-rich at the base of the core to organic-rich
407 above (Macumber et al., 2012). For Bridge Lake, the accumulation rate slows steadily
408 from a DT of ~50 yr/cm at 7,600 cal BP to c. 200 yr/cm at 4,000 cal BP. This
409 accumulation rate change is linked to a distinct color change at ~4,200 cal BP, from light
410 grey below (Munsell code 5y 3/2) to brown (Munsell code 10yr 2/1) above (Macumber et
411 al., 2012). The DT is constant around 200 yr/cm until c. 2,500 cal BP and steadily
412 increases to c. 160 yr/cm by 100 cal BP.

413

414 The accumulation rate profile for Horseshoe Lake displayed the highest variability of any

studied profile. Modeled DT is high (c. 20 yr/cm) between 8,700 – 7,500 cal BP and then decrease to c. 225 yr/cm by 5,000 cal BP. The transition around 7,500 cal BP is associated with a shift from minerogenic-rich sediment at the core bottom to organic-rich sediment above. Stratigraphically above ~7,500 cal BP, the accumulation rate gradually increases; DT reaching c. 100 yr/cm by 3,000 cal BP, then decreasing to 150 yr/cm by 2,000 cal BP, and finally increases again to 60 yr/cm at the core top.

4.4 Sites with poor chronological constraint

Some sites do not easily fit into the three recognized categories, either due to lack of dating resolution (P39 and Slipper lakes) or because the accumulation profile is characterized by a dramatic shift in accumulation rate (Portage North, Queens, and McMaster; Fig. 4). P39, Portage North, and McMaster lakes all had one outlier – identified on an ad hoc basis – that fell between 5,000 and 4,000 cal BP (Fig. 3). For P39, the radiocarbon date at the top of the core was determined to be an outlier. Because the core was collected in only 110 cm water depth, upper lake sediments may have been disturbed due to freezing of ice to the sediment-water interface. No further research was undertaken on this core and accumulation rates were not estimated. Slipper Lake lacked sufficient chronological control (based on two ^{14}C dates and a ^{210}Pb profile) and was also omitted from calculations of accumulation rate.

5. Bayesian age-depth modeling with Bacon

The temporal and spatial variations identified above are used as prior information for three Bayesian age-depth models to demonstrate the power and robustness of this

438 approach. The age modeling procedure for Bacon is similar to that outlined in Blaauw
439 and Christen (2005), but more numerous and shorter sections are used to generate a more
440 flexible chronology (Blaauw and Christen, 2011, 2013). Radiocarbon age distributions
441 are modeled using the Student-*t* distribution, which produces calibrated distributions with
442 longer tails than obtained using the Normal model (Christen and Pérez, 2009). Due to the
443 longer tails on radiocarbon dates and a prior assumption of unidirectional sediment
444 accumulation, in most cases excluding outliers is not necessary when using Bayesian age
445 modeling. The cores from Waite, Danny's and Horseshoe lakes all have at least ten non-
446 outlying radiocarbon dates and were deemed suitable for Bayesian modeling with Bacon.
447
448 As this is a demonstration of the practical application of Bacon (version 2.2; Blaauw and
449 Christen, 2011, 2013), text in italics denotes the actual code typed in R (statistical
450 computing and graphics software). Bacon version 2.2 uses the currently most recent
451 calibration curve, IntCal13 (Reimer et al., 2013), and has an added feature of plotting
452 accumulation rate data with the *plot.accrate.depth()* and *plot.accrate.age()* functions. In
453 Section 6.3 we show a practical example of the accumulation rate plotting function.
454
455 Memory or coherence in accumulation rates along the core is a parameter that is defined
456 based on the degree to which the accumulation rate at each interval depends on the
457 previous interval. For example, the memory for modeling accumulation in peat
458 sediments should be higher than for lacustrine sediments because accumulation of peat in
459 peat bogs is less dynamic over time than the accumulation of sediments in a lake. Here
460 we used the memory properties from the lake example in Blaauw and Christen (2011;

461 *mem.strength=20* and *mem.mean=0.1*).

462

463 The accumulation rates (*acc.rate=*) for Waite and Danny's lakes were based on the DT
464 estimates from Section 4 (20, and 70, respectively). The accumulation shape
465 (*acc.shape=*) for the Waite Lake cores was set to 2, as suggested by Blaauw and Christen
466 (2011). The accumulation shape controls how much influence the accumulation rate will
467 have on the model. The default value of 2 is fairly low, thus the model has a fair amount
468 of freedom to adapt rates to what the data suggest. For the Danny's lake age model, the
469 accumulation shape was increased to a value of 20 to avoid perturbations in the model
470 caused by known outliers. The step size for Waite Lake was set to 5 cm, which is the
471 default for a lake (Blaauw and Christen, 2011). The Danny's lake age-depth model
472 required more flexibility due to the observed shifts in accumulation rate that are unlikely
473 to be the product of spurious radiocarbon ages (they are sustained changes coherent with
474 known climate events), so the step sizes was lowered to 2 cm.

475

476 Horseshoe Lake required the addition of a hiatus (*hiatus.depths=45, hiatus.mean=10*) in
477 order to produce a realistic, stable model. Because the hiatus accounts for the slowest
478 accumulation rates for the age-depth model (>150 yr/cm between c. 6000 – 4000 cal BP),
479 the portion of the model below the hiatus accumulates at moderate rate (*acc.mean=70,*
480 *acc.shape=2*) and the portion of the model above the hiatus rate (*acc.mean=20,*
481 *acc.shape=1*). The physical nature of this hiatus is explored in Section 6.2.

482

483 The resulting age-depth models are shown in Figure 5, along with plots that describe: (1)

484 the stability of the model (log objective vs. iteration); (2) the prior (entered by the user)
485 and posterior (resulting) accumulation rate, and; (3) the prior and posterior memory
486 properties. The Bayesian model from Waite Lake shows stable accumulation rates over
487 time, most likely because this core covers the latest Holocene, during which time climate
488 was relatively consistent (Karst-Riddoch *et al.* 2005; Rühland & Smol 2005; Miller *et al.*
489 2010). Danny's Lake also yielded a stable model, with the consideration that the weight
490 on accumulation rate was set very high. The Horseshoe Lake model ran fairly stable,
491 with a minor perturbation.
492
493 The prior and posterior probability diagrams for accumulation rate were fairly similar for
494 Waite and Danny's lakes, and for Horseshoe Lake, the posterior distribution for
495 accumulation rate is a combination of the two assigned rates. Waite and Danny's lakes
496 models both showed memory of around 0.25, which is higher than was assigned (0.1).
497 The Horseshoe Lakes model had far less memory than assigned, but this is because
498 memory falls to 0 across a hiatus.

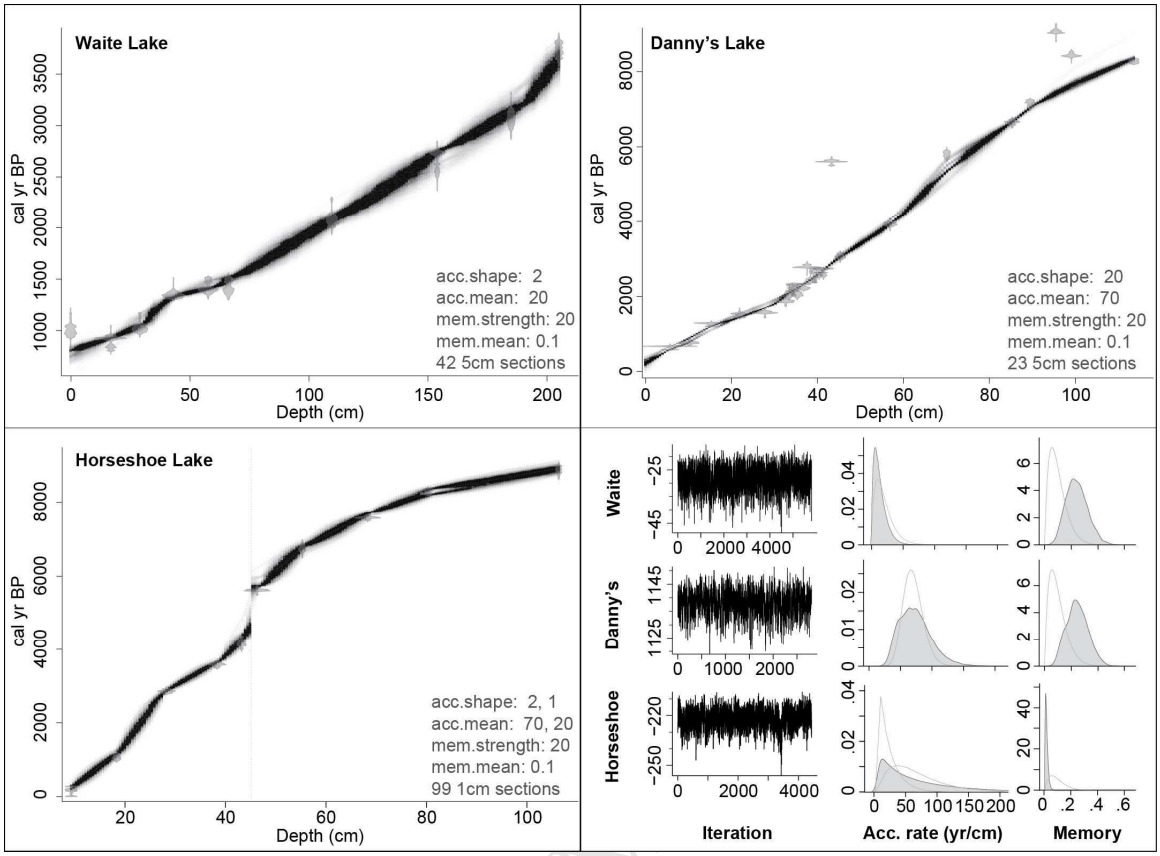

499

500

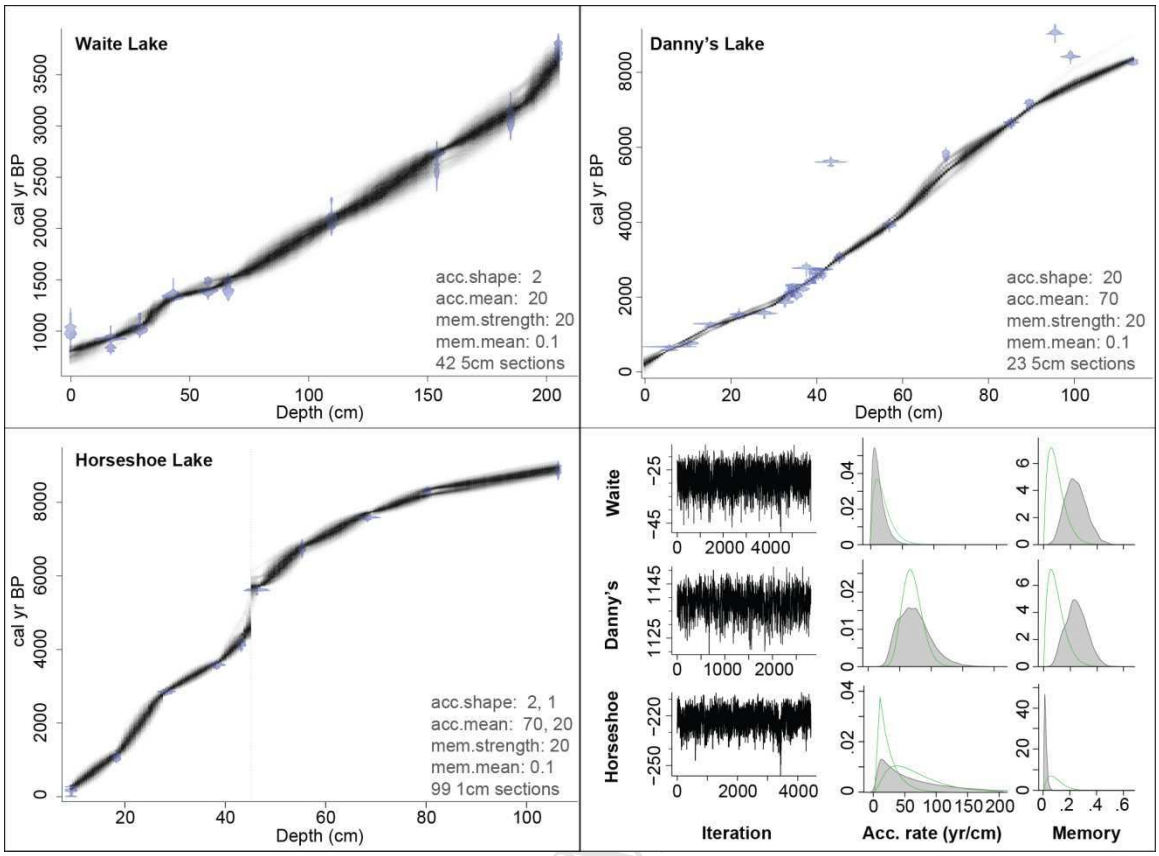

Figure 5. Bayesian age-depth models constructed with the age-depth modeling software Bacon for Waite, Danny's, and Horseshoe lake cores. The grayscale on the model represents the likelihood, where the darker the grey, the more likely the model is of running through that section. The vertical, dashed line on the Horseshoe Lake model denotes a hiatus. The bottom right panel shows three plots for each model: (left) stability of the model; (middle) prior (line) and posterior (filled) distributions of accumulation mean; and (right) prior (line) and posterior (filled) distributions of memory properties. ***Double column image. Colour version for web only. Black and white for print.***

6. Discussion

6.1 Spatial variability in accumulation rates

513 The three southernmost boreal forest lakes (Pocket, Tibbitt, and Waite) have the highest
514 accumulation rates, suggesting that the accumulation rate may be can be related to in-lake
515 productivity and in-wash of organic detritus. Sediment accumulation rates at Bridge and
516 Danny's lakes are slower than the more productive boreal lakes; Pocket, Tibbitt, and
517 Waite lakes. The last c. 3,000 years of accumulation at Danny's lake mirrors the pattern
518 of rapidly accumulating sites, but is slower by about a DT of 10-20 yr/cm. This suggests
519 that Danny's lake responded similarly to climate as the southernmost lakes, but may
520 either be slightly less productive due to colder temperatures at its location closer to the
521 polar front, or, judging by the bathymetry (Fig. 6), the coring site itself may receive less
522 sediment than the main basin of the lake, where sediment accumulation is most
523 commonly the greatest (c.f. Lehman, 1975). The accumulation rate at Bridge Lake is
524 extremely slow for the location south of the treeline and again we look at the bathymetry
525 for an explanation (Fig. 6). The coring location for Bridge Lake is nestled into a steep
526 slope, proximal to a deeper sub-basin with a much thicker sediment package. The slope
527 limits the amount of sediment that can accumulate at this site, and similarly to Danny's
528 Lake, much of the material is likely to have drifted toward the deeper basin.
529
530 Two of the most rapidly accumulating lakes are located in the tundra (Carleton-2012 and
531 Lac de Gras). Examination of the bathymetry profiles reveals certain basin features that
532 could explain the rapid accumulation rates (Fig. 6). Carleton Lake has a shallow shelf
533 over 500 m long that has a maximum depth of two meters, a slope covering less than 100
534 m, and a main basin that is about 500 m long at a depth of about 4 m (Fig. 6). The
535 Carleton-2012 freeze core was collected from a site closer to the slope and shelf than the

Carleton-1A and Carleton-1B freeze cores. The shelf, which is situated in two meters water depth, may be susceptible to re-suspension of fine detritus due to surface waves touching bottom generated during windy or stormy conditions. The re-suspended sediments would be transported down into the basin, with the majority being deposited closer to the slope terminus. A similar trend has been noted at two Lakes in Estonia whereby sediments deposited nearshore are thought to have eroded during a regressive period and redeposited elsewhere (Punning et al., 2007a, 2007b; Terasmaa, 2011). Looking at the bathymetry for Lac de Gras, it would be expected that since the coring site is steep, sediment would by-pass and be deposited in the deeper part of the lake. It is unclear, however, if there is a sub-basin at the coring site due to the low resolution of the available bathymetry (Fig. 6). The coring site was characterized by turbid water, steep surrounding landscape, and high minerogenic content of the core sediments (Macumber et al. 2012). Therefore, the rapid accumulation rate at this site is likely due to in-wash of material from the lake catchment. The other two cores from Lac de Gras (DM1 and DM3) are in a completely different sub-basin of the lake. These cores exhibit moderate to very slow accumulation rates, as would be expected on the tundra.

The Horseshoe lake core shows the highest variability in sedimentation rate of all the lakes. The core was extracted from a steep-sided sub-basin of the main lake (Fig. 6). The bathymetric profile is at a lower resolution than Bridge and Danny's lakes so it is not possible to determine exactly how the sediments drape over the bedrock. What is recognizable is that the sub-basin is only connected to the main basin by a shallow (0.5 m deep) passage. The sub-basin therefore would receive little direct sediment input from

559 snowmelt tributaries.

560

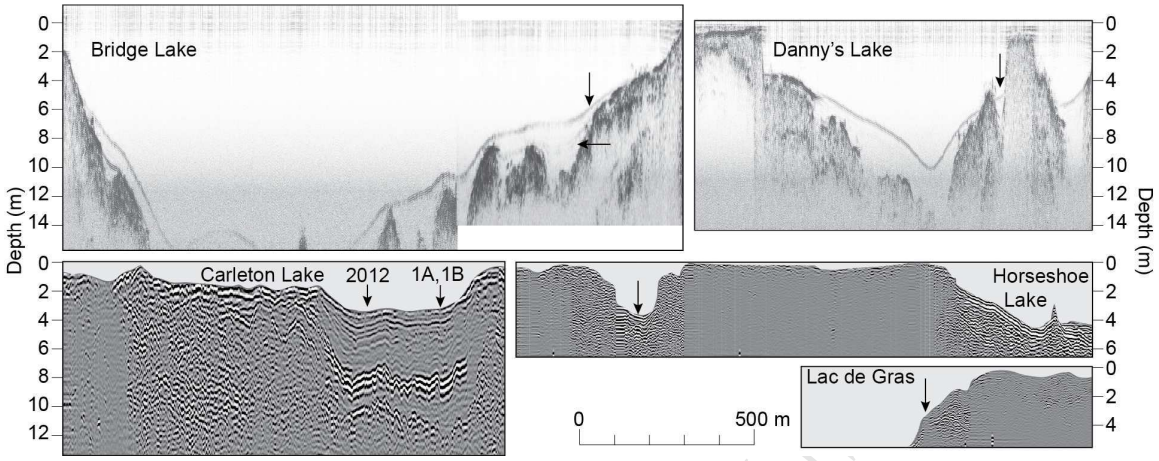

561

562 **Figure 6.** Bathymetry profiles from six lakes with arrows showing coring sites. The
563 horizontal arrow at Bridge Lake is pointing to a weak second reflector that is likely a
564 result of a change in sediment deposition from clay to gyttja, as observed in the core.
565 The coring site for Horseshoe Lake is in a sub-basin that is hydrologically connected to
566 the main basin through a meandering path as is shown in figure 3. ***Double column***
567 ***image.***

568

569 *6.2 Temporal variability in accumulation rates*

570 It is clear that the lakes in this region respond similarly during certain time periods (Fig.
571 4). It is also noteworthy that the density of radiocarbon dates has an influence on the
572 observed shifts in accumulation rate. For example, Danny's Lake and Horseshoe Lake
573 are well-dated cores (25 and 10 radiocarbon dates, respectively) and the accumulation
574 profiles are much more dynamic than most of the others. This is an important point
575 because it emphasizes that the first means of improving an age-depth model should
576 always be to add more radiocarbon dates. However, because radiocarbon dates are

577 expensive, it can be helpful to have an idea of when major shifts in accumulation rate for
578 a region are to be expected. That way, a more targeted approach can be employed when
579 refining an age-depth model using additional chronological control. Moreover, having an
580 idea of how the accumulation rate may shift over time for an age-depth model can assist
581 with identification of outliers as shown in section 3.3. Prior to a radiocarbon analysis,
582 major shifts in accumulation rate can be determined either visually (changes in sediment
583 composition) or by relatively inexpensive methods such as loss on ignition, magnetic
584 susceptibility, or palynology.
585
586 Seven of the ten cores that extend past about 7,000 cal BP show rapid accumulation rates
587 (DT ~50 yr/cm) at the base of their record and for nearly all these sites this is an above
588 average accumulation rate (Fig. 4). This rapid accumulation rate then steadily decreases
589 until c. 5,000 cal BP when most lakes with well-constrained age-depth models display the
590 slowest accumulation rates. At all seven sites, this occurs just after a transition from
591 minerogenic-rich sediment at the bottom to organic-rich sediment at the top (Fig. 7).
592 This is a common phenomenon in paraglacial environments when sediment availability
593 following glaciation is relatively high as long due to the presence of unstable drift
594 material in fluvial pathways (e.g. Church and Ryder, 1972; Ballantyne, 2002). Sediment
595 availability decreases as it is deposited, but also erosion rates are tempered as vegetation
596 is established (Huang et al., 2004). Results from an exponential exhaustion model by
597 Ballantyne (2002) support a decreasing accumulation rate over time as unstable sediment
598 is deposited. Briner et al. (2010) attribute the transition from minerogenic-rich to
599 organic-rich sediments to be indicative of the catchment for a proglacial lake getting cut

off from a nearby glacier. While most cores show a gradual colour change toward the basal sediments, the bottom 1 cm of Bridge Lake is composed of light grey clay that was likely deposited in just such a proglacial setting. We also see evidence for this shift in sediment type at Bridge Lake when looking at the bathymetry profile (Fig. 6), which shows a weak, second reflector near the bottom of the core site. Around the transition from minerogenic-rich sediments to organic-rich sediments, most lakes are characterized by slowest accumulation rates, coeval with a period of treeline advance in the region (Kaufman et al., 2004 and references therein). Similar relationships were noted for a lake in the Cathedral Mountains of British Columbia (Evans and Slaymaker, 2004) and in a crater lake in equatorial East Africa (Blaauw et al. 2011), whereby vegetation cover is thought to slow terrestrial erosion and allochthonous sediment supply to lakes due to physical stabilization of surficial materials. Following treeline advance, the accumulation rates in cores with the highest dating resolution (Danny's, Carleton-1B, and Horseshoe lakes) begin to increase again during late Holocene Cooling.

The accumulation rates for the cores from Lac de Gras, Carleton-2012 Lake, and Danny's Lake increase sharply between 1,500 cal BP and 1,300 cal BP, creating a small dip toward increased accumulation rates (Fig. 4, 7). Anderson et al. (2012) also found an increase in mineral accumulation rates at inland and coastal sites from c. 1,200 to 1,000 cal BP on southwest Greenland. They attribute this shift to regional cooling, increased aridity, and increased delivery of allochthonous material to the lake. At Carleton Lake, a cooling event between c, 1,690 and c. 940 cal BP is inferred based on chironomid proxy data (Upiter et al., 2014) and is temporally correlative with the timing of First Millennial

623 Cooling, a period of cool climatic conditions in the Northern Hemisphere and
624 documented in records from British Columbia (Reyes et al., 2006), Alaska (Hu et al.,
625 2001; Reyes et al., 2006; Clegg et al., 2010), and the Canadian Arctic Archipelago
626 (Thomas et al., 2011). Increased accumulation rates between c. 1,500 and c. 1,300 cal BP
627 may therefore correspond to cooling in the central NWT that would have resulted in a
628 brief period of reduced vegetation and consequently, increased erosion.

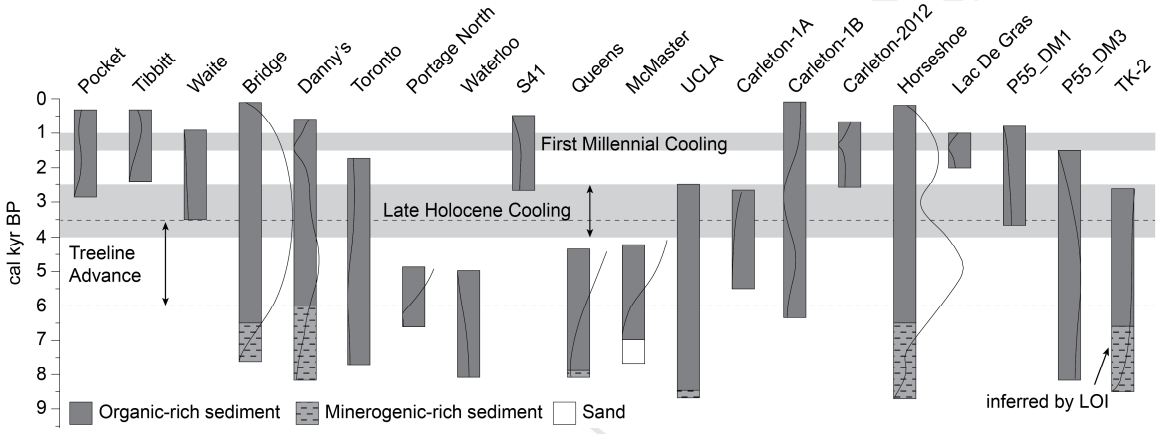

629

630 **Figure 7.** Stratigraphic core logs plotted against cal BP. The top of each core is defined
631 by the uppermost non-outlying radiocarbon date. Curved lines are accumulation profiles
632 from Fig. 4b and are to be interpreted left to right is faster to slower. Time ranges for the
633 treeline advance and Late Holocene Cooling follow Kaufman et al. (2004), and First
634 Millennial Cooling follows Reyes et al. (2006), Hu et al. (2001), Clegg et al. (2010), and
635 Thomas et al. (2011). ***Double column image.***

636

637 *6.3 Accumulation rate (DT) prior*

638 In Section 6.1 and 6.2, accumulation rates are discussed in terms of the natural
639 environment, which is a critical first step in any modeling study. In this section, we
640 switch gears to discuss the practical application of accumulation rates as prior

641 information for age-depth modeling with Bayesian statistics.

642

643 The default DT prior for Bacon version 2.2 is 20 yr/cm based on the estimate from the
644 great lakes region by Goring et al. (2012). Bacon version 2.2 is programmed to suggest
645 an alternative DT based on round values (e.g. 10, 50, 100 yr/cm) if the default of 20
646 yr/cm is inappropriate for the core. As was shown for Waite Lake, 20 yr/cm is an
647 appropriate estimate for most lakes found in the boreal forest zone, but lakes north of the
648 treeline accumulated at much slower rates. Here we use estimates from a summary of
649 accumulation rate data for the region to construct the age-depth models in section 5. The
650 most striking feature of these age-depth models is how variable the accumulation rate
651 appears to be. Figure 8 (constructed using the *plot.acc.rate()* function in Bacon 2.2)
652 shows a more detailed version of accumulation rate patterns for the three cores from
653 Section 5. Waite Lake only covers the past c. 3,500 years so variability is minimal, but
654 both the longer Danny's and Horseshoe Lake records display highly variable
655 accumulation rates (as discussed in Section 6.2). The estimates for accumulation rate
656 entered *a priori* into the model therefore act as a guide for the age-depth model, but do
657 not control the model entirely.

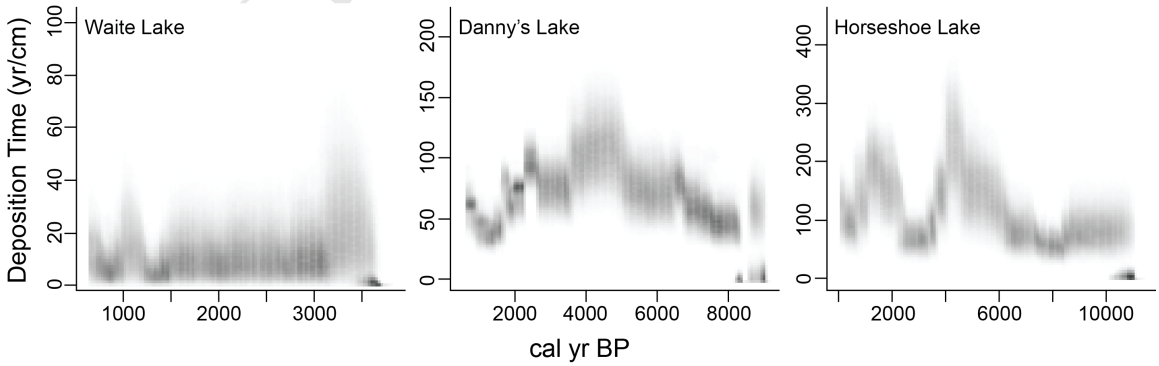

658

659 **Figure 8.** Accumulation profiles plotted with Bacon v2.2. The darker the grey, the

greater the certainty. ***Double column image.***

When an age-depth model is well dated, the dates themselves should guide the accumulation rate. In sections of the core with low dating resolution or age reversals, the Bayesian model can aid by incorporating prior information (Christen, 1994; Buck et al., 1996; Buck and Millard, 2004; Blaauw and Heegaard, 2012). Here we compare the Bayesian models to the Clam models in order to evaluate the effect of incorporating prior information. Because the Clam models were initially constructed with IntCal09, we reconstructed the models with IntCal13 order to ensure consistency (Supplementary Fig. 1). Moreover, a hiatus was added at 45 cm to the Horseshoe Lake model constructed with Clam. Differences between the maximum probability age of the Bayesian model and non-Bayesian model for Waite Lake, Danny's Lake, and Horseshoe Lake are presented in Figure 9.

Waite Lake has the simplest chronology, with only one distinguishable shift in accumulation rate just before c. 1,500 cal BP. The difference between the Bayesian and non-Bayesian models is 90 years at the most, which is minimal. For Danny's Lake, the difference between the two models is also fairly minimal (175 years at the most), which happens near the bottom of the model where the greatest uncertainty lies.

The difference between Bayesian and non-Bayesian age depth models for the Horseshoe Lake record does not tend to exceed 200 years, except in the region of the hiatus between c. 6,000 and c. 4,000 cal BP (45 cm), where the difference is 468 years. This is to be

683 expected as the hiatus is handled slightly differently between the two programs and it
684 causes a major disturbance in the model. C/N ratios from Horseshoe Lake suggest that
685 the sub-basin of Horseshoe Lake has undergone fluctuations in water depth (Griffith,
686 2013). Therefore, it is possible that there is a hiatus in deposition between c. 6,000 and c.
687 4,000 cal BP. A hiatus would also explain the anomalously slow accumulation rates
688 around this period as shown in figure 4.
689
690 Although not shown in Figure 9, the age-depth models constructed with Bacon have
691 wider and more realistic calculated error ranges than for the smooth spline models
692 constructed with Clam.
693

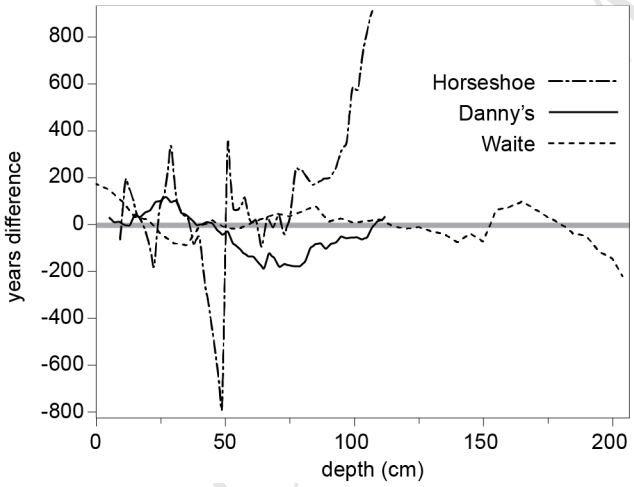

694

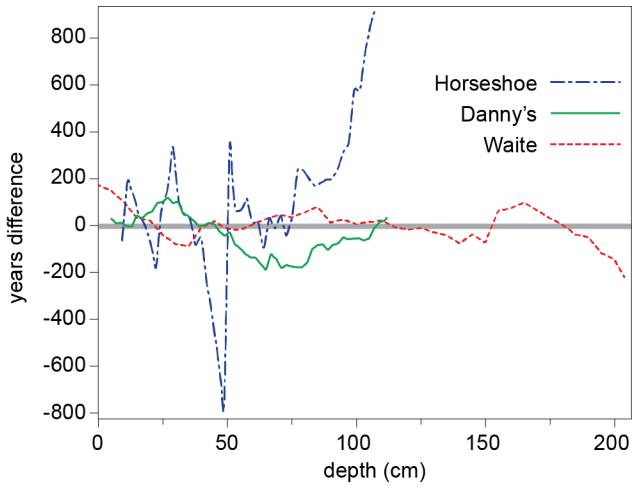

695

696 **Figure 9.** Plot showing the difference (in years) versus depth between the models

697 constructed in Clam and Bacon for the Horseshoe, Danny's and Waite Lake cores.

698 ***Single column image. Color for web version only.***

699

700 **7. Conclusions**

701 High resolution sampling and detailed age dating of subarctic lake cores from the

702 Northwest Territories have provided new information about the spatial and temporal

703 variability in lake accumulation rates in this cold, high latitude region. Based on a

704 dataset comprised of 105 radiocarbon dates (64 new and 41 previously published) from

705 22 sites distributed amongst 18 lakes, we make the following conclusions:

706 (1) "Rapid" accumulation rates (DT ~20 yr/m) tend to occur in lakes with high

707 productivity (boreal forest zone) or high sediment availability. Sites north of the treeline

708 are characterized by moderate (DT ~70yr/cm) to slow (DT >100 yr/cm) accumulation

709 rates with high spatial variability.

710 (2) Temporal shifts in accumulation rates coincide with centennial to millennial-scale

711 climate change and the waxing and waning of vegetation cover, which is an important

712 mechanism controlling erosion of material into lakes. Accumulation rates prior to about

713 7,000 cal BP were rapid, reflecting recently deglaciated conditions characterized by high
714 sediment availability and low vegetation cover. As vegetation became better established
715 during the treeline advance, we observed a shift from minerogenic-rich to organic-rich
716 sediments and a decrease in accumulation rates between 7,000 and 4,000 cal BP. This
717 was followed by a cool period and increasing accumulation rates between 4,000 cal BP
718 and 2,500 cal BP.
719 (3) Deposition time estimates from this research will be useful as a starting point for
720 building robust age-depth models using Bayesian statistics and state-of-the-art software
721 such as Bacon. Moreover, by elucidating the timing of regional shifts in accumulation
722 rate for the Canadian Subarctic, future radiocarbon dating sampling strategies will be
723 better informed about where to add additional radiocarbon dates to an age-depth model.
724

725 **Acknowledgements**

726 Funding for this collaborative research project was provided by a Natural Sciences and
727 Engineering Research Council of Canada (NSERC) Strategic Project Grant and
728 Discovery Grant to RTP and an Ontario Graduate Scholarship to CC. Direct and in-kind
729 funding was provided by the Northwest Territories Geoscience Office, Polar Continental
730 Shelf Project, the Department of Aboriginal Affairs and Northern Development Canada
731 (by, in part, a Cumulative Impacts and Monitoring Program award to JMG), the
732 Geological Survey of Canada, the Tibbitt to Contwoyto Winter Road Joint Venture (Erik
733 Madsen and the crew of the Dome, Lockhart, and Lac de Gras maintenance camps), EBA
734 Engineering Consultants Ltd., the North Slave Métis Alliance, IMG Golder, Inuvik, and
735 Golder Associates, Yellowknife.

736
737 **References**
738 Abbott, M.B., Stafford, T.W., 1996. Radiocarbon geochemistry of modern and ancient
739 Arctic lake systems, Baffin Island, Canada. Quaternary Research 45, 300–311. doi:
740 10.1006/qres.1996.0031
741
742 Anderson, N.J., Liversidge, A.C., McGowan, S., Jones, M.D., 2012. Lake and catchment
743 response to Holocene environmental change: spatial variability along a climate gradient
744 in southwest Greenland. Journal or Paleolimnology 48, 209–222. doi: 10.1007/s10933-
745 012-9616-3
746
747 Aravena, R., Warner, B.G., MacDonald, G.M., Hanf, K.I., 1992. Carbon isotope
748 composition of lake sediments in relation to lake productivity and radiocarbon dating.
749 Quaternary Research 37, 333–345. doi: 10.1016/0033-5894(92)90071-P
750
751 Ballantyne, C.K., 2002. Paraglacial geomorphology. Quaternary Science Reviews 21,
752 1935–2017. doi: 10.1016/S0277-3791(02)00005-7
753
754 Barnekow, L., Possnert, G., Sandgren, P., 1998. AMS ^{14}C chronologies of Holocene lake
755 sediments in the Abisko area, northern Sweden – a comparison between dated bulk
756 sediment and macrofossil samples. GFF 120, 59–67. doi: 10.1080/11035899801201059
757 Blaauw, M., 2010. Methods and code for 'classical' age-modeling of radiocarbon
758 sequences. Quaternary Geochronology 5, 512–518. doi: 10.1016/j.quageo.2010.01.002
759
760 Blaauw, M., 2010. Methods and code for 'classical' age-modeling of radiocarbon
761 sequences. Quaternary Geochronology 5, 512–518. doi: 10.1016/j.quageo.2010.01.002
762
763 Blaauw, M., Christen, J.A., 2005. Radiocarbon peat chronologies and environmental
764 change. Applied Statistics 54, 805–816. doi: 10.1111/j.1467-9876.2005.00516.x
765
766 Blaauw, M., Christen, J.A., 2011. Flexible paleoclimate age-depth models using an
767 autoregressive gamma process. Bayesian Analysis 6, 457–474. doi:
768 10.1214/ba/1339616472
769
770 Blaauw, M., Christen, J.A., 2013. Bacon manual – v2.2. 11 pp. Last accessed February
771 28, 2014 at http://www.chrono.qub.ac.uk/blaauw/bacon.html.
772
773 Blaauw, M., van Geel, B., Kristen, I., Plessen, B., Lyaruu, A., Engstrom, D.R., van der
774 Plicht, J., Verschuren, D., 2011. High-resolution 14C dating of a 25,000-year lake-
775 sediment record from equatorial East Afric. Quaternary Science Reviews 30, 3043–3059.
776 doi: 10.1016/j.quascirev.2011.07.014
777
778 Blaauw, M., Heegaard, E., 2012. Estimation of age-depth relationships. In: Birks, H.J.B.,
779 Lotter, A.F., Juggins, S., Smol, P., (Eds.), Tracking Environmental Change Using Lake
780 Sediments. Data Handling and Numerical Techniques. Vol. 5. Springer, Netherlands, pp.
781 379–413. doi: 10.1007/978-94-007-2745-8_12

Blass, A., Bigler, C., Grosjean, M., Sturm, M., 2007. Decadal-scale autumn temperature reconstruction back to AD 1580 inferred from the varved sediments of Lake Silvaplana (southeastern Swiss Alps). Quaternary Research 68, 184–195. doi: 10.1016/j.yqres.2007.05.004

Bleeker, W., 2002. Archaean tectonics: a review, with illustrations from the Slave craton. Geological Society of London, Special Publications 199, 151–181. doi: 10.1144/GSL.SP.2002.199.01.09

Blockley, S.P.E., Blaauw, M., Bronk Ramsey, C., van der Plicht, J., 2007. Building and testing age models for radiocarbon dates in Lateglacial and Early Holocene sediments. Quaternary Science Reviews 26, 1915–1926. doi: 10.1016/j.quascirev.2007.06.007

Briner, J.P., Stewart, H.A.M., Young, N.E., Philipps, W., Losee, S., 2010. Using proglacial-threshold lakes to constrain fluctuations of the Jakobshavn Isbræ ice margin, western Greenland, during the Holocene. Quaternary Science Reviews 29, 3861–3874. doi: 10.1016/j.quascirev.2010.09.005

Bronk Ramsey, C., 2009a. Dealing with outliers and offsets in radiocarbon dating. Radiocarbon 51, 1023–1045.

Bronk Ramsey, C., 2009b. Bayesian analysis of radiocarbon dates. Radiocarbon 51, 337–360.

Buck, C.E., Cavanagh, W.G., Litton C.D., 1996. Bayesian approach to interpreting archaeological date. Wiley, Chichester.

Buck, C.E., Millard, A.R. (Eds.), 2004. Tools for constructing chronologies: crossing disciplinary boundaries. Springer-Verlag, London. doi: 10.1007/978-1-4471-0231-1

Charman , D.J., Beilman, D.W., Blaauw, M., Booth, R.K., Brewer, S., Chambers, F.M., Christen, J.A., Gallego-Sala, A., Harrison, S.P., Hughes, P.D.M., Jackson, S.T., Korhola, A., Mauquoy, D., Mitchell, F.J.G., Prentice, I.C., van der Linden, M., De Vleeschouwer, F., Yu, Z.C., Alm, J., Bauer, I.E., Corish, Y.M.C., Garneau, M., Hohl, V., Huang, Y., Karofeld, E., Le Roux, G., Loisel, J., Moschen, R., Nichols, J.E., Nieminen, T.M., MacDonald, G.M., Phadtare, N.R., Rausch, N., Sillasoo, Ü, Swindles, G.T., Tuittila, E.-S., Ukonmaanaho, L., Välliranta, M., van Bellen, S., van Geel, B., Vitt, D.H., Zhao, Y., 2013. Climate-related changes in peatland carbon accumulation during the last millennium. Biogeosciences 10, 929-944 www.biogeosciences.net/10/929/2013/

Christen, J.A., 1994. Bayesian interpretation of radiocarbon results. Ph.D. thesis, University of Nottingham.

Christen, J.A., Pérez E.S., 2009. A new robust statistical model for radiocarbon data. Radiocarbon 51, 1047–1059.

Church, M., Ryder, J.M., 1972. Paraglacial sedimentation: a consideration of fluvial processes conditioned by glaciation. Geological Society of America Bulletin 83, 3059–3072. doi: 10.1130/0016-7606(1972)83[3059:PSACOF]2.0.CO;2

Clayton, J.S., Ehrlich, W., Cann, D.B., Day, J.H., Marshall, I.B., 1977. Soils of Canada. Soil Inventory Research Branch, Canada, vol. II. Department of Agriculture, Ottawa. 239 pp.

Clegg, B.F., Clarke, G.H., Chipman, M.L., Chou, M., Walker, I.R., Tinner, W., Hu, F.S., 2010. Six millennia of summer temperature variation based on midge analysis of lake sediments from Alaska. Quaternary Science Reviews 29, 3308–3316. doi: 10.1016/j.quascirev.2010.08.001

Cockburn, J.M.H., Lamoureux, S.F., 2008. Inflow and lake controls on short-term mass accumulation and sedimentary particle size in a High Arctic Lake: implications for interpreting varved lacustrine sedimentary records. Journal of Paleolimnology 40, 923–942. doi: 10.1007/s10933-008-9207-5

Crann, C., 2013. Spatial and temporal variability of lake accumulation rates in Subarctic Northwest Territories, Canada. MSc thesis, Carleton University.

Dyke, A.S., Prest, V.K., 1987. Late Wisconsinan and Holocene history of the Laurentide Ice Sheet. Géographie Physique et Quaternaire 41, 237–263. doi: 10.7202/032681ar

Dyke, A.S., Moore, A., Robertson, L., 2003. Deglaciation of North Americ. Geological Survey of Canada Open File, 1574. doi: 10.4095/214399

Evans, M., Slaymaker, O., 2004. Spatial and temporal variability of sediment delivery from alpine lake basins, Cathedral Provincial Park, southern British Columbia. Geomorphology 61, 209–224. doi: 10.1016/j.geomorph.2003.12.007

Galloway, J.M., Macumber, A.L., Patterson, R.T., Falck, H., Hadlari, T., Madsen, E., 2010. Paleoclimatological assessment of the southern Northwest Territories and implicatons for the long-term viability of the Tibbitt to Contwoyto Winter Road, part 1: core collection. Northwest Territories Geoscience Office, NWT Open Report 2010-002, 21 p.

Geyh, M.A., Schotterer, U., Grosjean, M., 1998. Temporal changes of the 14C reservoir effect in lakes. Radiocarbon 40, 921–931.

Glew, J.R., 1991. Miniature gravity corer for recovering short sediment cores. Journal of Paleolimnology 5, 285–287. doi: 10.1007/BF00200351

Glew, J.R., Smol, J.P., Last, W.M., 2001. Sediment core collection and extrusion. In: Last, W.M., Smol, J.P. (Eds.), Tracking environmental changes using lake sediments:

874 Volume 1: Basin analysis, coring and chronological techniques. Dordrecht: Kluwer
875 Academic Publishers p 73–105.
876
877 Goring, S., Williams, J.W., Blois, J.L., Jackson, S.T., Paciorek, C.J., Booth, R.K.,
878 Marlon, J.R., Blaauw, M., Christen, J.A., 2012. Accumulation rates in the northeastern
879 United States during the Holocene: establishing valid priors for Bayesian age models.
880 Quaternary Science Reviews 48, 54–60. doi: 10.1016/j.quascirev.2012.05.019
881
882 Grimm, E.C., Maher Jr., L.J., Nelson, D.M., 2009.The magnitude of error in conventional
883 bulk-sediment radiocarbon dates from central North Americ. Quaternary Research 72,
884 301–308. doi: 10.1016/j.yqres.2009.05.006
885
886 Helmstaedt, H., 2009. Crust-mantle coupling revisited: The Archean Slave craton, NWT,
887 Canada. Lithos 112S, 1055–1068. doi: 10.1016/j.lithos.2009.04.046
888
889 Hu, F.S., Ito, E., Brown, T.A., Curry, B.B., Engstrom, D.R., 2001. Pronounced climatic
890 variations in Alaska during the last two millennia. Proceedings of the National Academy
891 of Sciences 98, 10552–10556. doi: 10.1073/pnas.181333798
892
893 Hua, Q., Barbetti, M., 2004. Review of tropospheric bomb 14C data for carbon cycle
894 modeling and age calibration purposes. Radiocarbon 46, 1273–1298.
895
896 Hua, Q., Barbetti, M., Rakowski, A.Z., 2013. Atmospheric radiocarbon for the period
897 1950-2010. Radiocarbon 55, doi:10.2458/azu_js_rc.v55i2.16177

898 Huang, C.C., MacDonald, G., Cwynar, L., 2004. Holocene landscape development and
899 climatic change in the low arctic, Northwest Territories, Canada. Palaeogeography,
900 Palaeoclimatology, Palaeoecology 205, 221–234. doi: 10.1016/j.palaeo.2003.12.009
901
902 Karst-Riddoch, T., Pisaric, M. & Smol, J., 2005, Diatom responses to 20th century
903 climate-related environmental changes in high-elevation mountain lakes of the northern
904 Canadian Cordillera. Journal of Paleolimnology 33, 265–282.
905
906 Kaufman, D.S., Ager, T.A., Anderson, N.J., Anderson, P.M., Andrews, J.T., Bartlein,
907 P.J., Brubaker, L.B., Coats, L.L., Cwynar, L.C., Duvall, M.L., Dyke, A.S., Edwards,
908 M.E., Eisner, W.R., Gajewski, K., Geirsdóttir, A., Hu, F.S., Jennings, A.E., Kaplan,
909 M.R., Kerwin, M.W., Lozhkin, A.V., MacDonald, G.M., Miller, G.H., Mock, C.J.,
910 Oswald, W.W., Otto-Bliesner, B.L., Porinchu, D.F., Rühland, K., Smol, J.P., Steig, E.J.,
911 Wolfe, B.B., 2004. Holocene thermal maximum in the western Arctic (0–180 W).
912 Quaternary Science Reviews 23, 529–560. doi: 10.1016/j.quascirev.2003.09.007
913
914 Koff, T., Punninga, J.-M., Kangura, M., 2000. Impact of forest disturbance on the pollen
915 influx in lake sediments during the last century. Review of Palaeobotany and Palynology
916 111, 19–29. doi: 10.1016/S0034-6667(00)00013-0
917

Kulbe, T., Niederreiter Jr., R., 2003. Freeze coring of soft surface sediments at a water depth of several hundred meters. Journal of Paleolimnology 29, 257–263. doi: 10.1023/A:1023209632092

Lehman, J., 1975. Reconstructing the rate of accumulation of lake sediment: the effect of sediment focusing. Quaternary Research 5, 541–550. doi: 10.1016/0033-5894(75)90015-0

Lerbekmo, J.F., 2008. The White River Ash: largest Holocene Plinian tephra. Canadian Journal of Earth Sciences 45, 693–700. doi: 10.1139/E08-023

Lotter, A.F., Renberg, I., Hansson, H., Sto□ckli, R., Sturm, M., 1997. A remote controlled freeze corer for sampling unconsolidated surface sediments. Aquatic Sciences 59, 295–303.

MacDonald, G.M., Edwards, T.W.D., Moser, K.A., Pienitz, R., Smol, J.P., 1993. Rapid response of treeline vegetation and lakes to past climate warming. Nature 361, 243–246. doi: 10.1038/361243a0

MacDonald, G.M., Porinchu, D.F., Rolland, N., Kremenetsky, K.V., Kaufman, D.S., 2009. Paleolimnological evidence of the response of the central Canadian treeline zone to radiative forcing and hemispheric patterns of temperature change over the past 2000 years. Journal of Paleolimnology 41, 129–141. doi: 10.1007/s10933-008-9250-2

Macumber, A.L., Patterson, R.T., Neville, L.A., Falck, H., 2011. A sledge microtome for high resolution subsampling of freeze cores. Journal of Paleolimnology 45, 307–310. doi: 10.1007/s10933-010-9487-4

Macumber, A.L., Neville, L.A., Galloway, J.M., Patterson, R.T., Falck, H., Swindles, G., Crann, C., Clark, I., Gammon, P., Madsen, E., 2012. Paleoclimatological assessment of the Northwest Territories and implications for the long-term viability of the Tibbitt to Contwoyto Winter Road, part II: March 2010 field season results. Northwest Territories Geoscience Office, NWT Open Report 2011-010, pp. 83.

Marlon, J., Bartlein, P.J., Whitlock, C., 2006. Fire-fuel-climate linkages in the northwestern USA during the Holocene. The Holocene 16, 1059–1071. doi: 10.1177/0959683606069396

Miller, G., Brigham-Grette, J., Alley, R., Anderson, L., Bauch, H., Douglas, M., Edwards, M., Elias, S., Finney, B., Fitzpatrick, J., Funder, S., Herbert, T., Hinzman, L., Kaufman, D. S., MacDonald, G. M., Polyak, L., Robock, A., Serreze, M., Smol, J., Spielhagen, R., White, J., Wolfe, A. & Wolff, E., 2010. Temperature and precipitation history of the Arctic. Quaternary Science Reviews 29, 1679–1715.

963 Moser, K.A., MacDonald, G.M., 1990. Holocene vegetation change at treeline north of
964 Yellowknife, Northwest Territories, Canada. Quaternary Research 34, 227–239. doi:
965 10.1016/0033-5894(90)90033-H
966
967 Oana, S., Deevey, E.S., 1960. Carbon 13 in lake waters and its possible bearing on
968 paleolimnology. American Journal of Science 258, 253–272.
969
970 Padgham, W.A., Fyson, W.K., 1992. The slave province: a distinct Archean craton.
971 Canadian Journal of Earth Science 29, 2072–2086. doi: 10.1139/e92-165
972
973 Paul, C.A., Ru□hland, K.M., Smol, J.P., 2010. Diatom-inferred climatic and
974 environmental changes over the last ~9000 years from a low Arctic (Nunavut, Canada)
975 tundra lake. Palaeogeography, Palaeoclimatology, Palaeoecology 291, 205–216.
976
977 Pientiz, R., Smol, J.P., MacDonald G.M., 1999. Paleolimnological reconstruction of
978 Holocene climate trends from two boreal treeline lakes, Northwest Territories, Canada.
979 Arctic, Antarctic, and Alpine Research 31, 82–93. doi: 10.2307/1552625
980
981 Pyne-O'Donnell, S.D.F., Hughes, P.D.M., Froese, D.G., Jensen, B.J.L., Kuehn, S.C.,
982 Mallon, G., Amesbury, M.J., Charman, D.J., Daley, T.J., Loader, N.J., Mauquoy, D.,
983 Street-Perrott, F.A., Woodman-Ralph, J., 2012. High-precision ultra-distal Holocene
984 tephrochronology in North Americ. Quaternary Science Reviews 52, 6–11. doi:
985 10.1016/j.quascirev.2012.07.024
986
987 Punning, J.-M., Koff, T., Sakson, M., Kangur, M., 2007a. Holocene pattern of organic
988 carbon accumulation in a small lake in Estonia. Polish Journal of Ecology 55,
989 5–14.
990
991 Punning, J.-M., Boyle, J.F., Terasmaa, J., Vaasma, T., Mikomägi, A., 2007b. Changes in
992 lake sediment structure and composition caused by human impact: repeated studies of
993 Lake Martiska, Estonia. The Holocene, 17, 145–151. doi: 10.1177/0959683607073297
994 Rampton, V.N., 2000. Large-scale effects of subglacial meltwater flow in the southern
995 Slave Province, Northwest Territories, Canada. Canadian Journal of Earth Science 37,
996 81–93. doi: 10.1139/e99-110
997
998 Reimer, P.J., Brown, T.J., Reimer, R.W., 2004. Discussion: reporting and calibration of
999 post-bomb 14C data. Radiocarbon 46, 1299–1304.
1000
1001 Reimer, P.J., Baillie, M.G.L., Bard, E., Bayliss, A., Beck, J.W., Blackwell, P.G., Bronk
1002 Ramsey, C., Buck, C.E., Burr, G.S., Edwards, R.L., Friedrich, M., Grootes, P.M.,
1003 Guilderson, T.P., Hajdas, I., Heaton, T.J., Hogg, A.G., Hughen, K.A., Kaiser, K.F.,
1004 Kromer, B., McCormac, F.G., Manning, S.W., Reimer, R.W., Richards, D.A., Southon,
1005 J.R., Talamo, S., Turney, C.S.M., van der Plicht, J., Weyhenmeyer, C.E., 2009. IntCal09
1006 and Marine09 radiocarbon age calibration curves, 0-50,000 years cal BP. Radiocarbon
1007 51, 1111–1150.
1008

Reimer, P.J., Bard, E., Bayliss, A., Beck, J.W., Blackwell, P.G., Bronk Ramsey, C., Buck, C.E., Cheng, H., Edwards, R.L., Friedrich, M., Grootes, P.M., Guilderson, T.P., Haflidason, H., Hajdas, I., Hatté, C., Heaton, T.J., Hoffmann, D.L., Hogg, A.G., Hughen, K.A., Kaiser, K.F., Kromer, B., Manning, S.W., Niu, M., Reimer, R.W., Richards, D.A., Scott, E.M., Southon, J.R., Staff, R.A., Turney, C.S.M., van der Plicht, J., 2013. IntCal13 and Marine13 Radiocarbon Age Calibration Curves 0–50,000 Years cal BP. Radiocarbon 55, 1869–1887. Doi: 10.2458/azu_js_rc.55.16947

Reyes, A.V., Wiles, G.C., Smith, D.J., Barclay, D.J., Allen, S., Jackson, S., Larocque, S., Laxton, S., Lewis, D., Calkin, P.E., Clague, J.J., 2006. Expansion of alpine glaciers in Pacific North America in the first millennium A.D. Geology 34, 57–60. doi: 10.1130/G21902.1

Robinson, S.D., 2001. Extending the late Holocene White River Ash distribution, Northwestern Canada. Arctic 54, 157–161.

Rühland, K., Smol, J.P., 2005. Diatom shifts as evidence for recent Subarctic warming in a remote tundra lake, NWT, Canada. Palaeogeoprahy, Palaeoclimatology, Palaeoecology 226, 1–16. doi: 10.1016/j.palaeo.2005.05.001

Saulnier-Talbot, E., Pienitz, R., Stafford Jr., T.W., 2009. Establishing Holocene sediment core chronologies for northern Ungava lakes, Canada, using humic acids (AMS 14C) and 210Pb. Quaternary Geochronology 4, 278–287. doi: 10.1016/j.quageo.2009.02.018

Schiefer, E., 2006. Contemporary sedimentation rates and depositional structures in a montane lake basin, southern Coast Mountains, British Columbia, Canada. Earth Surface Processes and Landforms 31, 1311–1324. doi: 10.1002/esp.1332

Smith, D.G., 1994. Glacial Lake McConnell: paleogeography, age, duration, and associated river deltas, Mackenzie River Basin, Western Canada. Quaternary Science Reviews 13, 829–843. doi: 10.1016/0277-3791(94)90004-3

Stephenson, S.R., Smith, L.C., Agnew, J.A., 2011. Divergent long-term trajectories of human access to the Arctic. Nature Climate Change 1, 156–160. doi: 10.1038/nclimate1120

Stuiver, M., 1975. Climate versus changes in 13C content of the organic components of lake sediments during the late Quaternary. Quaternary Research 5, 251–262. doi: 10.1016/0033-5894(75)90027-7

Stuiver, M., Polach, H.A., 1977. Discussion: reporting of 14C data. Radiocarbon 19, 355–363.

Stuiver, M., Reimer, P.J., 1993. Extended 14C database and revised Calib 3.0 14C age calibration program. Radiocarbon 35, 215–230.

Terasmaa, J., 2011. Lake basin development in the Holocene and its impact on the sedimentation dynamics in a small lake (southern Estonia). Estonian Journal of Earth Sciences, 60(3), 159–171. doi: 10.3176/earth.2011.3.04

Thomas, E.K., Briner, J.P., Axford, Y., Francis, D.R., Miller, G.H., Walker, I.R., 2011. A 2000-yr-long multi-proxy lacustrine record from central Baffin Island, Arctic Canada reveals first millennium AD cold period. Quaternary Research 75, 491–500. doi: 10.1016/j.yqres.2011.03.003

Upiter, L.M., Vermaire, J.C., Patterson, R.T., Crann, C., Galloway, J.M., Macumber, A.L., Neville, L.A., Swindles, G.T., Falck, H., Roe, H.M., Pisaric, M.F.J., in review. A mid- to late Holocene chironomid-inferred temperature reconstruction for the central Northwest Territories, Canada. Journal of Paleolimnology.

Webb, R.S., Webb, T., 1988. Rates of sediment accumulation in pollen cores from small lakes and mires of eastern North America. Quaternary Research 30, 284–297. doi: 10.1016/0033-5894(88)90004-X

Wedel, J.H., Smart, A., Squires, P., 1990. An overview study of the Yellowknife river basin, N.W.T. N.W.T. programs: inland waters directorate conservation and protection. Western and Northern Region, Environment Canada, Ottawa.

Wolfe, B.B., Edwards, T.W.D., Aravena, R., MacDonald, G.M., 1996. Rapid Holocene hydrologic change along boreal tree-line revealed by δ13C and δ18O in organic lake sediments, Northwest Territories, Canada. Journal of Paleolimnology 15, 171–181. doi: 10.1007/BF00196779

Wright Jr., R.G., Mann, D.H., Glaser, P.H., 1984. Piston cores for peat and lake sediments. Ecology 65, 657–659. doi: 10.2307/1941430

a) Waite Lake

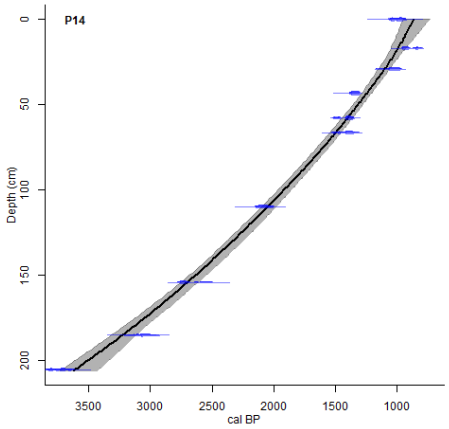

b) Danny's Lake

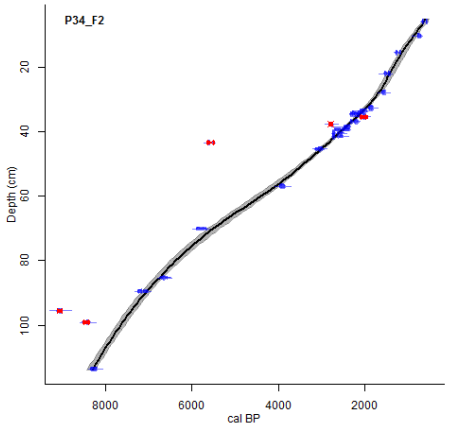

c) Horseshoe Lake

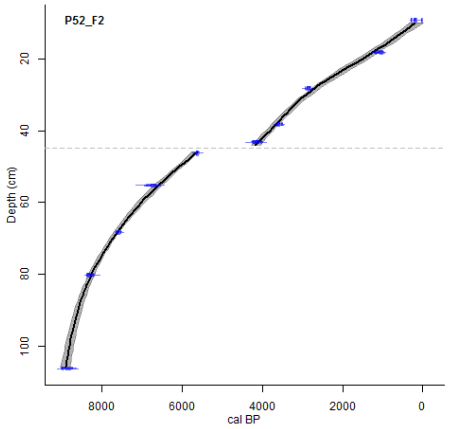

Supplementary Figure 1. Smooth spline age-depth model constructed for: a) Waite Lake; b) Danny's Lake; and c) Horseshoe Lake using the age-depth modeling software Clam and the IntCal13 calibration curve. For Horseshoe Lake, a hiatus is shown with a dashed line at 45 cm